Collisional Studies of Ultracold Cesium

Thesis by

Joshua L. Bliss

In Partial Fulfillment of the Requirements

for the Degree of

Doctor of Philosophy

California Institute of Technology

Pasadena, California

1999

(Submitted September 2, 1998)

Acknowledgements

A number of people deserve specific mention for their long term and deep involvement in the work of this thesis. First is my advisor Professor Ken Libbrecht, who has given me the opportunity to work in such an interesting field and shared his considerable knowledge of laboratory techniques with me, both by demonstration and explanation.

Also, erstwhile graduate students Richard Boyd and Phil Willems deserve special note. Between them they designed and constructed much of the cryotraps version 1 and 2 and so much of everything else in the cryotrapping laboratory in which much of my research was done. My close working relationship in the lab with Rich and Phil was a great education in experimental physics. My ongoing scientific conversations with Phil have also been both enjoyable and important to my progess. Richard also convinced me that C++ can be useful , such as the code he left me, but he has failed to convince me that he will ever beat me at Duke Nukem.

Thank you also to James Kohel, Robert Thompson, Dave Siedel, and Lute Maleki at the Time and Frequency Standards Division of JPL. James and Rob in particular have spent long and late hours with me in the lab and are the best collaborators one could ask for.

I also thank Professor Jeff Kimble and his Quantum Optics group for the extensive use of their chemistry room and other facilities and the frequent loans of equipment, as well as all the technical advice from many past and current members of the group, in particular David Vernooy and Jun Ye with whom I had many enlightening and interesting discussions, and who always showed patience answering my questions.

I am also indebted to my officemates Eric Black, Robert Cameron, and Shanti Rao, who have aided me with design problems, proofread parts of this thesis, and otherwise helped me on a regular basis.

Much of the machining on the beam source elements was done by Ricardo Paniagua.

I gratefully acknowledge the financial support of Millard Jacobs, whose generous contribution made cryotrap version 2 possible.

I especially thank my parents, whose unwavering support of my education my entire life has allowed me to reach this point.

Also, I would like to thank all the wonderful friends I've made while at Caltech, with whom I've had so much fun these years. In particular, those not mentioned already include Patrick Brady, Samya Habuni, David Hill, Scott Hughes, Fredrick Jenet, and Ben Owen.

Abstract

Spin-polarized neutral cesium atoms are confined in a magnetostatic trap in a cryogenic apparatus. The atoms are prepared in the $F = 4, m_F = 4$ state and cooled, with rf-assisted evaporative cooling, to less than 10 microKelvin.

The elastic scattering cross section is measured by disequilibrating magnetostatically trapped atoms and observing the rate of equilibration. A computer simulation is presented, the results of which are used to extract the elastic scattering cross section from the measured rates of equilibration. For cesium atoms in the $F = 4, m_F = 4$ state, the elastic cross section is confirmed to have a resonant magnitude which varies inversely with the mean kinetic energy, implying a scattering resonance.

A design for a new beam source of cold neutral atoms, based on an optical funnel with a pyramid mirror configuration, is also presented.

Contents

List of Figures

Chapter 1 Introduction

1.1 General Introduction and Summary

In the last decade, the trapping and cooling of atoms with lasers and magnets has become an increasingly important and common tool in atomic physics. Samples of neutral atoms with temperatures of a few tens of a millionth of a Kelvin and densities in excess of 10^9atoms/ cm^3 can now be readily produced in laboratories around the world. This has provided a high-density source of cold atoms for many experiments in atomic physics. For example, the use of a magneto-optical trap (MOT) allows improved accuracy in precision atomic measurements, such as atomic cesium clocks, that were previously limited by the high velocity and relatively low density of effusive thermal atomic beams.

Another line of research enabled by laser trapping and cooling has been the production of even colder and denser neutral atomic samples by evaporative cooling. This line of research achieved a milestone in 1995 with the observation of Bose-Einstein Condensation (BEC) in atomic gases of rubidium [1] and sodium [2]. The cryogenic atom trap at Caltech, which had already demonstrated very long trap lifetimes due to ultralow background pressures, and very strong magnetic confinement produced by superconducting coils in close proximity to the trap center, was well suited to perform evaporative cooling experiments. Chapter 2 describes the apparatus including the magnetic coils and the laser sources.

We began by evaporatively cooling samples of cesium in the $|F = 4, m_F = 4\rangle$ state [3], and found we were unable to efficiently evaporatively cool the atoms below about $7\,\mu$K despite an apparently large elastic cross section. To try to understand this, we measured the cross section at a range of temperatures. Prior to our experiments, Tiesinga *et al.* [4], working from phase shifts measuerd in atomic fountain experiments, had produced a hypothesis that in the low temperature limit, cesium in the

$|F = 4, m_F = 4\rangle$ state had a very large elastic cross section. Such a large cross section would fall off as $1/T$ for a wide range of temperatures, including temperatures typical for magnetostaticly-trapped cesium (from a few μK to a few hundred μK). Some of the theory behind this behavior, and how it can be observed, is covered in Chapter 3. Chapter 4 contains the experimental procedure and the data analysis as well as a set of simulations which were necessary to interpret the data. Söding *et al.* [5] have recently published a set of careful observations demonstrating that at low temperatures there is a giant spin relaxation for cesium in the $|F = 4, m_F = 4\rangle$ state which prevents further efficient evaporative cooling in this state. Our results are consistent with this.

In Chapter 5 a new intense beam of slow and cold atoms design is presented. This beam had been constructed and is awaiting final testing at Jet Propulsion Laboratory (JPL). This beam would be an asset to cryotrapping, where it could in principle increase the lifetime of magnetostatic traps by several times. However, the beam is first destined for other experiments at JPL which require an intense, slow, and cold beam.

1.2 Introduction

Laser cooling and trapping is the source of cold atoms for all of the experiments described in this thesis. The basic aspects of laser cooling and trapping will be reviewed in this section. A more comprehensive introduction can be found in review articles by Lett *et al.* [6] and by Dalibard *et al.* [7].

1.2.1 Doppler Cooling

The basic idea behind laser cooling is straightforward. If a single near-resonant laser beam (i.e., traveling wave) of wavevector $\overrightarrow{k}$ interacts with a two-level atom with natural linewidth Γ moving at velocity $\overrightarrow{v}$, the atom will absorb and reemit photons

at a rate of

$$\gamma_+ = \frac{\Gamma}{2}\frac{I}{I_{sat}}\left(\frac{1}{I/I_{sat}+1+(4/\Gamma^2)(\delta-\overrightarrow{k}\cdot\overrightarrow{v})^2}\right), \tag{1.1}$$

where I is the intensity of the laser beam, I_{sat} is the saturation intensity of the atomic transition, and δ is the detuning of the laser from the resonant frequency of the transition, ω_0 (i.e., $\delta = \omega_{\text{laser}} - \omega_0$). The $\overrightarrow{k}\cdot\overrightarrow{v}$ term represents the additional detuning the laser atoms sees due to the Doppler shift of the laser's frequency in the atom's rest frame. For notational simplicity, let us call v the component of the velocity of $\overrightarrow{v}$ in the $-\widehat{k}$ direction.

Every absorption of a photon by the atom causes an impulse on the atom of $\hbar k$ along $\widehat{k}$. The reemission of a photon by the atom is isotropic and random and causes no average force (although the variance of these impulses will cause heating). Thus the time averaged force on the atom is $\hbar k\gamma_+$. If δ is chosen to be negative and two counter-propagating lasers are used, then the scattering rate from the two beams is γ_+ and γ_- respectively, and the force is

$$\begin{aligned} F &= \hbar k(\gamma_+ - \gamma_-) = \\ &\frac{\Gamma}{2}\frac{I}{I_{sat}}\left(\frac{1}{I/I_{sat}+1+(4/\Gamma^2)(\delta-kv)^2} - \frac{1}{I/I_{sat}+1+(4/\Gamma^2)(\delta+kv)^2}\right) \end{aligned} \tag{1.2}$$

is a damping force in that the sign of the force is opposite the sign of kv. This force arises because of the first order Doppler effect, and is often called Doppler cooling. The force becomes linear with-respect-to velocity when the laser intensity is low, i.e., $I/I_{sat} \ll 1$, and v is small enough that $kv \ll \delta$. Then $F = -\alpha v$ where $\alpha = 2\hbar k^2\delta(I/I_{sat})/(1+4(\delta/\Gamma)^2)^2$.

An atom in this light field will also experience heating due to momentum diffusion from the isotropically distributed random reemissions. The minimum theoretical temperatue occurs when $\delta = -\Gamma/2$ and this temperature is called the Doppler temperature, $T_D = \hbar\Gamma/2k_{\text{Boltz}}$.

For cesium, the cycling transition $6S_{1/2,F=4} \longrightarrow 6P_{3/2,F=5}$ is used for cooling and

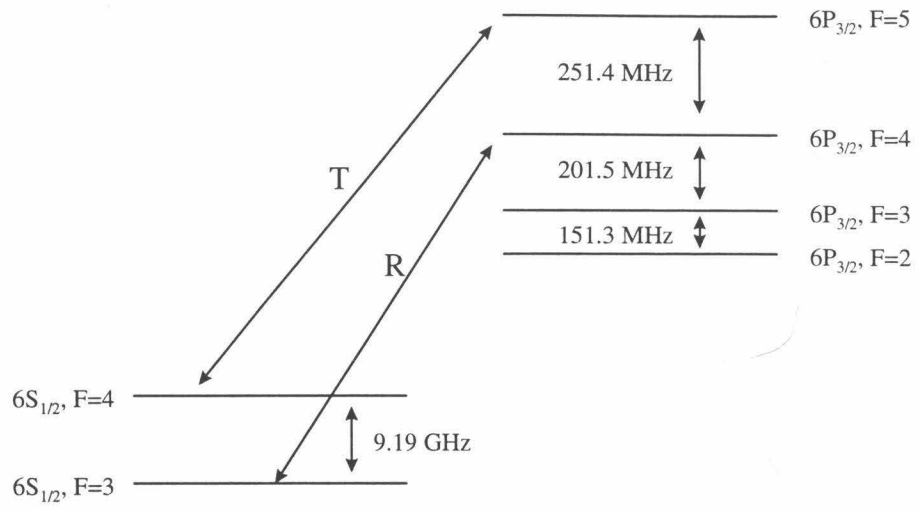

Figure 1.1: Hyperfine levels of cesium used for laser cooling. T is the trapping transition. R is the repumping transition.

trapping. The level diagram for the $6S_{1/2}$ and $6P_{3/2}$ levels is shown in figure 1.1. The transition labeled T is the trapping transition and corresponds to approximately 852.36 nm (vacuum). For this transition I_{sat} is 1.1 mW and $\Gamma = 2\pi \times 5.1$ MHz. Off resonant excitation of the $6S_{1/2,F=4} \longrightarrow 6P_{3/2,F=4}$ transition, which is about 250 MHz away from the trapping transition, allows atoms to optically pump into the $6S_{1/2,F=3}$ groundstate, which is 9.2 GHz lower than the $6S_{1/2,F=4}$ state. In order to put these atoms back into the cooling cycle, a so-called repumping laser is added, which is tuned to the $6S_{1/2,F=3} \longrightarrow 6P_{3/2,F=4}$ state, labeled R in the figure.

1.2.2 Magneto-Optical Trapping

If the above system of Doppler cooling is extended to three dimensions using six laser beams, a cloud of atoms will form at the intersection of the beams. Because the force on the atoms is viscous, this cloud is called an optical molasses. However, this cloud of atoms is just cooled, not trapped. The cloud forms because the time required for atoms from the background gas to cross the molasses region has been increased. To actually confine atoms for more than the fraction of a second they take to move

through the molasses region, a restoring force is required. A simple and powerful way to produce this restoring force is the Magneto-Optical Trap (MOT), sometimes called a Zeeman-Shift Optical Trap (ZOT).

In a MOT, a spatially varying magnetic field causes a spatially varying Zeeman shift in the atomic states involved in the laser cooling. The magnetic field usually used is a simple quadrupole field as created between two circular current loops running with opposite currents (figure 1.2). In one dimension, this field is $B = bz$ near the center. Consider the simplest theoretical case of cooling with a $J = 0 \rightarrow 1$ transition in one dimension, using two counter-propagating lasers as for an optical molasses. The ground state $J = 0$ has no Zeeman shift, but the excited state will divide into $m_J = \{-1, 0, 1\}$ Zeeman levels. A σ^+ beam will be able to excite atoms into the $m = 1$ excited state and a σ^- beam will be able to excite atoms into the $m = -1$ state. The effect of the magnetic field $B = bz$ is to shift the $J = 1, m = 1$ state to higher energy for positive z and to lower energy for negative z, and the opposite for the $J = 1, m = -1$ state (figure 1.3). If the lasers are tuned below the resonant frequency of the transition ($\delta < 0$), as for an optical molasses, then the effect of this Zeeman shift will be to make the atoms absorb more photons from the σ^- beam in the region with positive magnetic field and from the σ^+ beam in the region with negative magnetic field. If the σ^- beam is chosen to come from the direction of increasing magnetic field, a restoring force towards the $B = 0$ point in the middle will be established, in addition to the damping force from the Doppler cooling. The actual MOT is three-dimensional, and the $F = 4 \rightarrow F = 5$ transition of cesium has additional complications arising from additional energy levels compared to the model of the simple $J = 0 \longrightarrow 1$ transition.

1.2.3 Real MOTs

The MOT would be expected to have about the same minimum temperature as the optical molasses, $T_D \approx 120\,\mu\text{K}$. The actual temperatures measured in cesium MOTs can be much lower, as low as about $1\,\mu\text{K}$ or even less. This is sometimes called

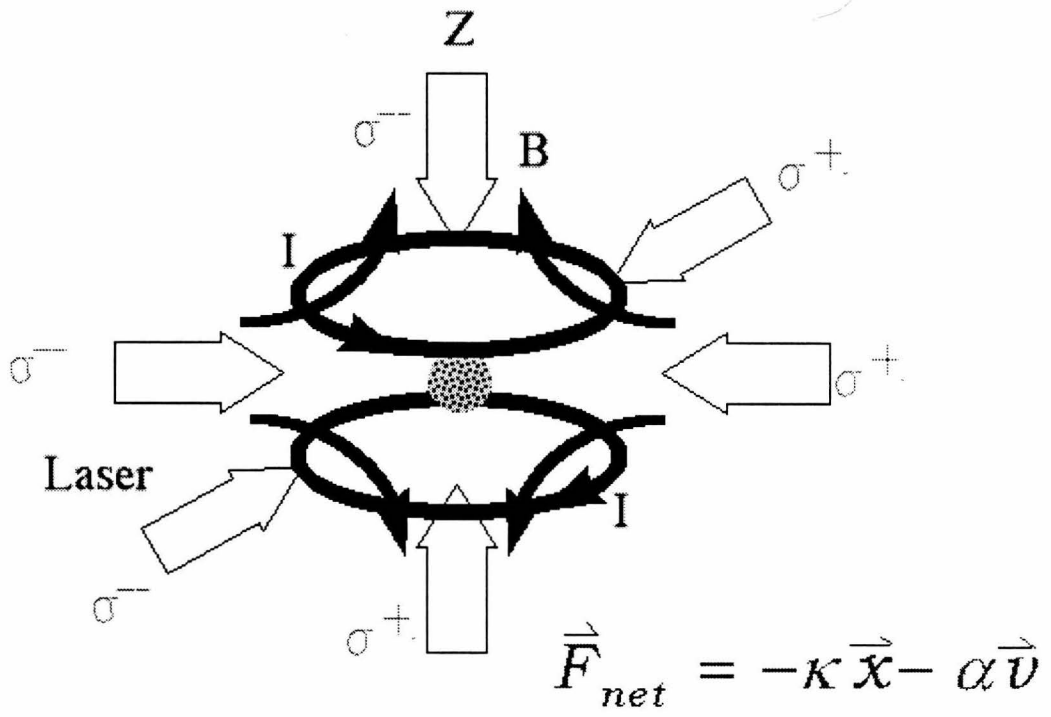

Figure 1.2: The configuration of lasers, currents, and magnetic fields for a standard 6 beam MOT.

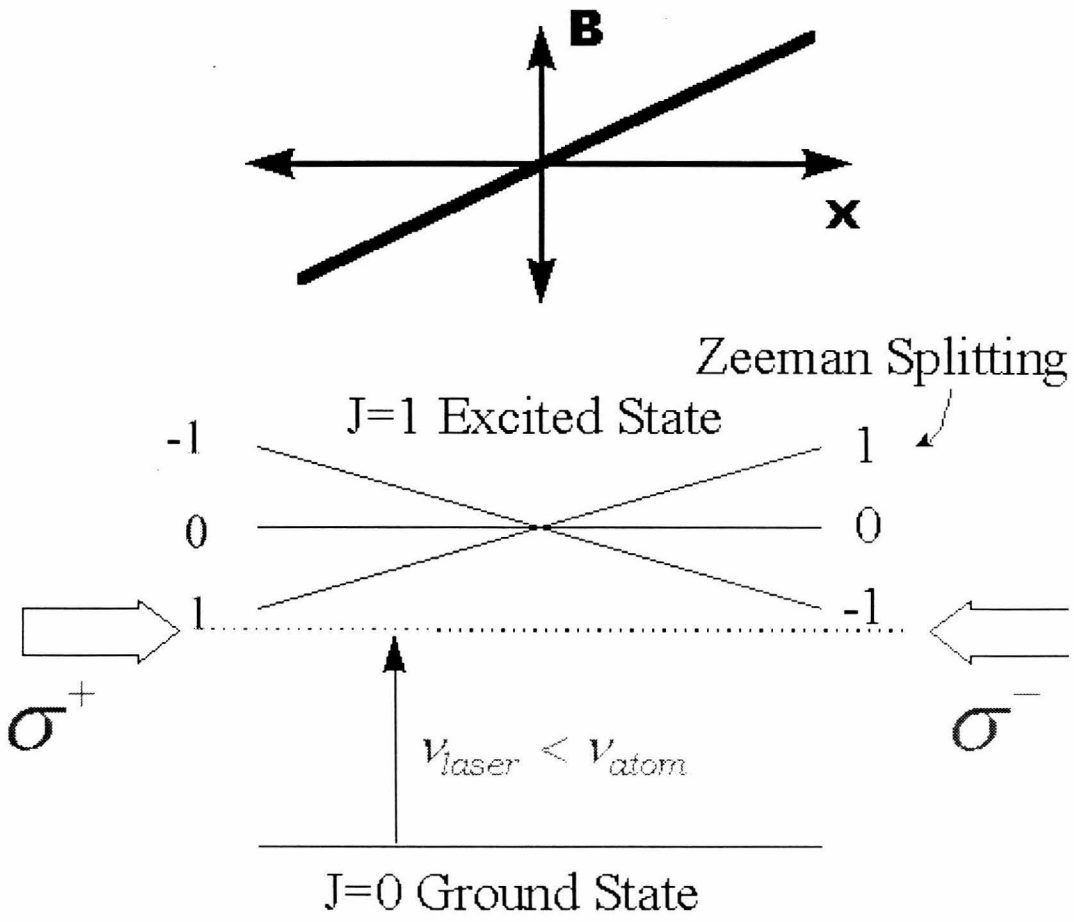

$$\Rightarrow F_{net} = -\kappa x - \alpha v_x$$

Figure 1.3: A one-dimensional MOT.

sub-Doppler cooling, and arises from the multi-level structure of the atoms. The mechanisms for sub-Doppler cooling depend on the polarization gradient present in the laser field. That is, the polarization of the combined laser field changes in space. A discussion of how this spatial dependence of the polarization causes sub-Doppler cooling is beyond the scope of this introduction. A discussion can be found in the previously mentioned review articles [6][7].

The appropriate limit for the lowest achievable temperatures in a three-dimensional MOT is about the energy of a single photon recoil, $k_B T_{\text{recoil}} = \hbar^2 k^2 / 2m$, which is about $0.1\,\mu$K for cesium. In our system, we are attempting to maximize the density in the MOT in order to increase the collision rate after the atoms are loaded into the magnetostatic trap. This increased density, and the need to keep the lasers and magnetic fields optimized to capture many atoms, keep our MOT temperatures around 10 to $30\,\mu$K.

Chapter 2 Apparatus

2.1 Introduction

The collisional studies described in this thesis were all carried out in a cryogenic ultrahigh vacuum system designed and built by our group for producing magneto-optical and magnetostatic traps. The cryogenic system does not change the essential physics of the interactions of atoms with near resonant light and magnetic fields, but there are significant experimental differences when compared to room temperature atom trapping and cooling. These differences are almost all in the vacuum system and the magnetic field coils, which are the topic of the first of the two sections of this chapter. The second section deals with the lasers, optics, and imaging required to produce the magneto-optical trap and to probe the magnetostatically trapped atoms.

2.2 Vacuum and Magnetic Coils

2.2.1 Vacuum System Including the Cesium Beam

The device used in these experiments, and its precursor [44] also constructed by the Libbrecht group at Caltech, are the only cryogenic atom traps constructed with MOT capability. Previous applications of atom trapping in a cryogenic environment were completely magnetostatic trapping of hydrogen [9] in dilution refrigerator and an early apparatus constructed by Pritchard which had only one dimension of optical access [10].

Both of the cryogenic atom traps at Caltech were primarily designed by Professor Libbrecht and two graduate students, Richard Boyd and Phil Willems. A thorough description of version 2, the apparatus used for the collision experiments in this thesis, can be found in Chapter 3 of Richard Boyd's thesis [3]. The schematic drawing in

figure 2.1 shows the vacuum chamber without the beam apparatus.

The source of cesium atoms was a thermal beam designed and built by Phil Willems which is discussed more fully in his thesis [8]. The beam begins with a cesium oven where a sample of cesium atoms is held at a temperature adjustable between 25 °C for no beam and 140 °C for maximum beam. The cesium atoms are partially collimated by passing through a multichannel glass capillary array of 2 mm thickness, 1 cm diameter open aperture, and 10 μm pore diameter (Galileo Electro-Optics Corp., part number C13S20M10) [11]. The beam enters the inner vacuum chamber through an interlock chamber, at the end of which a shutter allows the isolation of the inner chamber from the cesium beam during the longest trap lifetime experiments. The shutter consists of a polished copper plate that rests in a holder below the opening to the cesium beam when in the open position. The shutter is tied to a stainless steel weight in the interlock chamber by a Kevlar thread. The weight pulls the shutter closed by means of a pulley. A linear actuator lifts the weight to allow the shutter to fall into the open position.

When the shutter is open, the cesium beam is also the primary source of background atoms in the inner cryogenic vacuum chamber. The lifetime of the magnetostatic traps increased by typically more than a factor of 10 to as long as an hour when the beam shutter is closed, and the inner chamber has had a few minutes to achieve its final pressure of approximately a few 10^{-13} torr. Unfortunately, almost 90% of the atoms are typically lost in the first 8 minutes [8] after the shutter is closed. When the shutter mechanism failed during the early collision experiments, it was decided to be not worth breaking vacuum to repair it. The equilibration timescales, the important time scale for our collision experiments, were still much less than the trap lifetime, even with the beam shutter open for the entire experiment. Instead of fixing the shutter, the trap lifetime was maximized by operating the beam at a lower temperature, about 70 °C, and the atom number was brought back up by better optimizing the slower laser, as discussed in the second section of this chapter.

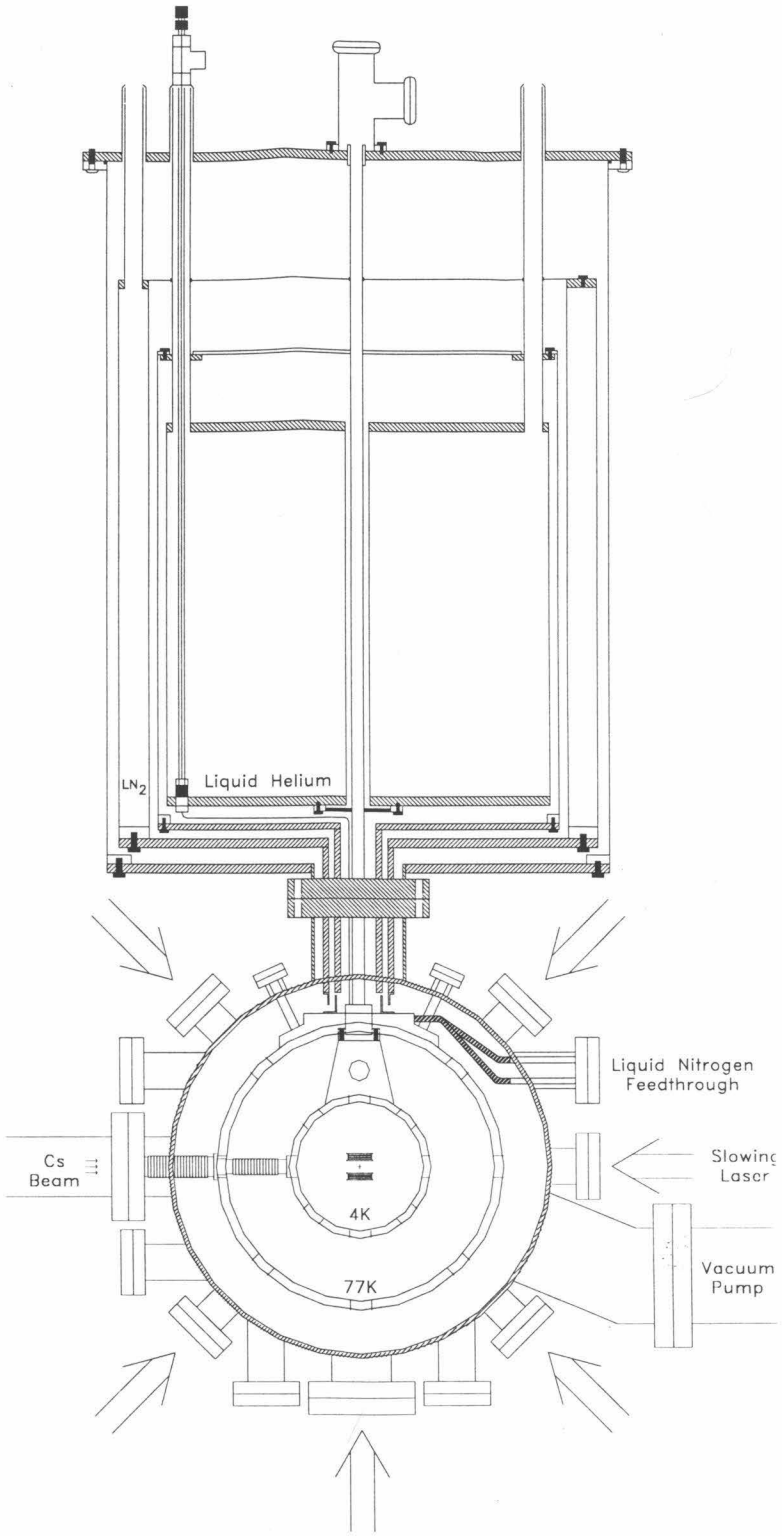

Figure 2.1: The cryotrapping system. The horizontal trapping laser beams and radiation shield tubes are shown rotated up 90° from the horizontal plane. The downward trapping laser beam enters horizontally and is reflected downward through the trap by a mirror inside the inner chamber.

2.2.2 Magnet Coils

The primary advantages of a cryogenic atom trapping are twofold. The first is that the inherently very good vacuum provided by a cryogenic vacuum system allows a very low trap loss rate from collisions with background gas atoms. This loss rate is a limiting factor to the efficiency of evaporative cooling and also impedes the measurement of slow processes such as dimensional equilibration, which is discussed in chapter 4. The second advantage is that cryogenics allow the use of superconducting magnets, which can produce large magnetic fields, gradients, and curvatures without additional cooling besides that already required to maintain the inner chamber near 3 K. The magnets can also be placed inside the inner vacuum chamber, just outside the area required for laser cooling beams. This allowed us to produce very large magnetic fields, field gradients, and field curvatures, with an adjustability not available with permanent magnets, and with field biases not available with conventional coils, except with kilowatts of dissipated power. The superconducting coil set was of the Ioffe/Yin-Yang family, with an additional pair of coils for magneto-optical trapping (figure 2.2), and is discussed by Richard Boyd [3].

Near the center, the coils produce a magnetic field given by

$$B = B_0 + \beta z^2 + G_z z + \frac{1}{2}\left(\frac{\alpha^2}{B_0} - \beta\right)\rho^2, \tag{2.1}$$

where ρ is the cylindrical radial coordinate $\rho = \sqrt{x^2 + y^2}$. In terms of the currents (in Amperes) in the four coils in the coil set [3], the coefficients are given by

$$\alpha = 200 I_{\mathrm{YY}}\ \mathrm{G/cm^2} \tag{2.2}$$

$$\beta = (20 I_{\mathrm{YY}} + 300 I_2 - 55 I_{\mathrm{Bias}})\ \mathrm{G/cm^2} \tag{2.3}$$

$$B_0 = (55 I_{\mathrm{YY}} + 279 I_2 - 705.6 I_{\mathrm{Bias}})\ \mathrm{G} \tag{2.4}$$

$$G_z = 870(I_1 - \frac{1}{2} I_2)\ \mathrm{G/cm^2}\,. \tag{2.5}$$

Each coil can handle up to about 10 amps of current, but we almost always limited the current to 5 amps or less.

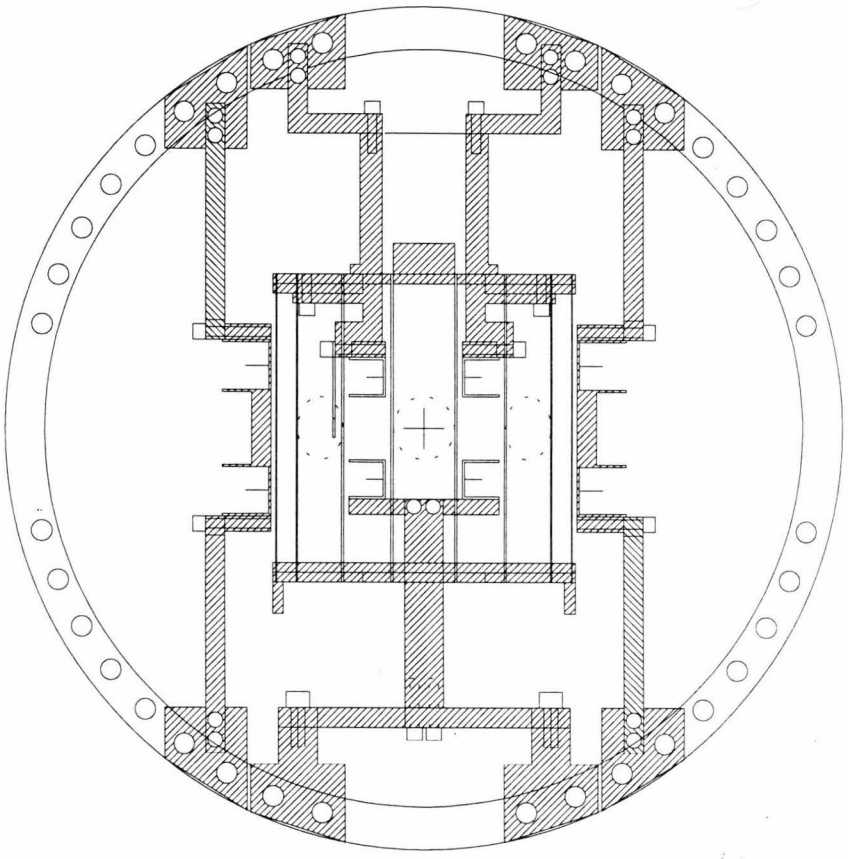

Figure 2.2: The coil form for the yin-yang coils at the MOT coils.

The atoms in this magnetic field see a total potential $U_{\text{total}} = \mu B + mgz$ where $\mu = \mu_{Bohr} g_F m_F$. That is,

$$U_{\text{total}} = \mu B_0 + \mu\beta z^2 + \mu\frac{1}{2}\left(\frac{\alpha^2}{B_0} - \beta\right)\rho^2 + (\mu G_z + mg)z. \tag{2.6}$$

Concerning the last term, which is linear in z, a linear potential added to a quadratic potential merely displaces the equilibrium position without changing the spring constant. Choosing the equilibrium position as the new origin is defining $\tilde{z} = z - (mg + \mu G_z)/(2\mu\beta)$. Discarding constant terms in the potential, U has only quadratic terms. This assumes that the trap stays harmonic as far as this from the geometric center of the trap, which needs to be calculated or measured independently. In practice, we usually choose G_z so as to cancel gravity. That is, so that $G_z = -mg/\mu$ and $\widetilde{z} = z$. In either case, the effective potential is

$$U = \mu\beta\widetilde{z}^2 + \left(\frac{\mu}{2}\right)\left(\frac{\alpha^2}{B_0} - \beta\right)\rho^2. \tag{2.7}$$

The spin-polarized, and weak-field seeking, states $|F = 4, m = 4\rangle$, for which $g_F m_F \approx 1$, and $|F = 3, m = -3\rangle$, for which $g_F m_F \approx 3/4$, are the states of interest here. This is primarily because these are the states which can be held in a magnetostatic trap without large losses from inelastic collisions. For those the states, the trap frequencies are, in Hz,

$$\nu_z = \frac{1}{\pi}\sqrt{\frac{\mu\beta}{2m}} = \begin{cases} 1.46\sqrt{\beta} \text{ for } (F = 4,\ m = 4) \\ 1.26\sqrt{\beta} \text{ for } (F = 3,\ m = -3) \end{cases} \tag{2.8}$$

$$\nu_\rho = \begin{cases} 1.03\sqrt{\left(\frac{\alpha^2}{B_0} - \beta\right)} \text{ for } (F = 4,\ m = 4) \\ 0.89\sqrt{\left(\frac{\alpha^2}{B_0} - \beta\right)} \text{ for } (F = 3,\ m = -3) \end{cases}. \tag{2.9}$$

2.3 Optics, Imaging, and Lasers

Laser cooling, trapping, and imaging requires a number of stabilized and tunable lasers, some of which must be modulated and shuttered on microsecond time scales.

Imaging also requires a camera and optical system with sufficient intensity and spatial resolution to analyze the spatial distribution of the atoms.

For laser sources, diode lasers were chosen for their well known advantages. They are easily available at 852 nm, relatively inexpensive (< \$500 for a 100 mW laser diode), compact and electrically efficient. Their linewidth can easily be narrowed to a few hundred kilohertz with optical feedback. Additionally they can be tuned and modulated with optical feedback, temperature changes, and laser drive current.

For the evaporative cooling and collision experiments, it was crucial to maximize the number of atoms in the trap without increasing the background pressure of cesium from the cesium beam. This was achieved with a chirped slowing laser, accompanied by a chirped repumper laser. These are in addition to the trapping laser, the repumping laser, and the master laser, whose electronics and optics in our system are described previously [3][8]. The atoms were imaged with an Apogee AP7 slow scan cooled CCD camera, which is based on an efficient SiTE model back illuminated CCD array. An overview of the laser and optical system follows, with special attention given to the slowing and slowing-repumper lasers as well as the modifications to the imaging system and procedure.

2.3.1 Laser Sources

The lasers used in this experiments were a mix of SDL-5413 and older STC LT50A03u lasers. We found the lifetime of the STC lasers was greatly shortened if they were operated at much more than half their rated powers, while several of the newer SDL lasers were operated at 80-90% of their rated power continuously for over a year without any failures.

By their nature, laser diodes are very stigmatic and divergent at their exit aperture. For a typical high power single-mode, index-guided diode laser, the emitting edge is about 1 μm by 3 μm in size, and the divergence is about 500 mrad and 170 mrad (half-cone) respectively. In principle, the extremely small emitting area implies that geometric optics allows the beam to be very well collimated when it is expanded to a

centimeter or two. For a typical final beam size of 1 cm diameter, the theoretical best collimation from geometric optics is a divergence of 50 μrad (half-cone). This level of collimation is neither easily attained, nor necessary for our experiment. We use a fast collimating compound lens (Melles Griot type 06 GLC 001 with 6.5 mm focal length) which collimates the output beam into an elliptical beam with a 4 : 1 aspect ratio, whose size is about a centimeter along the longer axis, with a divergence of a few milliradians. The beam is then circularized with an anamorphic prism pair. This was the most cost-effective collection and collimation of the diode laser light we could get with the then available commercial lens and the STC package. Currently one can do better, due in part to the newer standard SOT-148 type lower profile package used in the SDL lasers, and the ready availability of better collimation lenses. But the experiment did not require upgrading this part of the laser optics.

The collimating lens and the block containing the laser diode are situated in the mechanical laser housing, facing a 1800 lines/mm holographic grating (Edmund Scientific D43,221), mounted in the Littrow configuration, as described by MacAdams *et al.* [12]. (This grating was accidently reported to be 2400 lines/mm in Dr. Boyd's thesis). The source of external cavity feedback is the first order diffraction from this grating. The mechanical housing we developed for this whole assembly is discussed previously [8][3]. For the purposes of the research in this thesis, there are a few salient features of the mechanical housing. The diode laser's temperature is adjustable and stabilized to within 1 mK. The angle of the grating can be adjusted with both a manual screw for a gross tuning of the laser frequency over a range of about 2 THz while adjusting the temperature over the available range of a few Kelvins, and a piezoelectric crystal for finer laser frequency tuning over a range of a few GHz at a tuning rate of a few GHz / ms.

The drive current source used for these lasers is that of Libbrecht and Hall [13]. The source supplies up to 200 mA of current at a voltage compliance of about 10 V, with a temperature stability of approximately 1 μA / K and a current noise of less than 50 nA in a 1 MHz bandwidth. The current source also allows external (dc coupled) modulation of the current, as well as the direct addition of radio-frequency

modulation.

The method we used for locking and tuning the master laser, the trapping laser, and the repumping laser relative to atomic transitions in cesium were initially mostly unchanged from the scheme discussed in a previous thesis from our group [8]. Certain changes to the locking schemes were necessary for the later experiments working with the (F=3, m=-3) groundstate, and are mentioned in Chapter 4 describing these experiments.

For all the evaporative cooling experiments, the necessity of maximizing the number of atoms trapped without increasing the background pressure from the cesium beam required the addition of a so-called slowing-laser to enhance the fraction of the atoms from the cesium beam that could be captured in the MOT.

2.3.2 The Chirped Slower

The idea of slowing an atomic beam using an oppositely directed resonant laser beam is straightforward. In each optical absorption and emission cycle, the atom receives one photon worth of momentum in the laser beam's propagation direction and emits a photon in a random direction. The result of many such cycles is to slow the atom's motion along the beam. The emitted photons are expected to be uniform in direction as the atomic spins are randomly oriented (and the slowing beam is linearly polarized).

Although the total isotropic photon emissions by the atom will not increase the mean velocity in any direction, it will increase the root-mean-square (rms) velocity of the atom in the directions transverse to the laser beam. This is a random walk in velocity space, and the transverse rms velocity can be expected to increase as the square root of the number of optical cycles. This has been called transverse heating. In addition to this heating, the cesium beam will also increase in cross section as the transverse velocity spread of the beam is not decreased while the longitudinal velocity is. That is, the transit time to the trap center is doubled by the slowing, giving the transverse velocities twice as long to carry atoms away from the center of the beam.

These shortcomings can be overcome, somewhat, with techniques such as transverse laser cooling. However, for our experiments, the additional optical access required and the general increased complexity were not worth the increase in trap lifetime that would have resulted from being able to decrease the beam temperature even more.

The principal unignorable difficulty faced when slowing an atomic beam with a resonant laser beam is that the Doppler shift of the resonant frequency changes as the atoms are slowed. For instance, for a cesium atom starting at $v_i = 2 \times 10^4 \,\mathrm{cm\,/\,s}$, the velocity corresponding to the most probable velocity at 300 K, the initial Doppler shift is $v_i/\lambda = 235\,\mathrm{MHz}$. If the longitudinal velocity of the atom is to be reduced to a few meters per second or less, then the total change in the Doppler shift during the slowing is more than 40 times the natural linewidth of the optical transition. This is about the situation we faced. The distribution of the velocities of the atoms from our cesium beam is unknown, but the cesium oven was usually about 350 K, and the effect of the collimating array is, probably, to somewhat preferentially pass atoms with higher initial velocity along the channels which are therefore less likely to collide with the surface of the channel.

The challenge of keeping the atoms in resonance with the laser as they are slowed has been met in a number of ways by different groups. For instance, the optical transition can be broadened by interaction with an intense laser [14][15], the resonance itself can be shifted by different amounts at different points in space by an inhomogeneous magnetic [16][17] or electric [18] field, or a powerful laser can be frequency-broadened so that the atoms always see some light near resonance as they are slowed [19]. The earliest technique to compensate for decreasing Doppler shifts during slowing was that of frequency-chirping the slowing laser [20][21]. This technique is not optimal in the sense that not all of the atoms benefit from the slowing action. The beginning of the chirp of the slowing laser may or may not coincide with when a particular atom first emerges from the microchannel array. But frequency-chirped slowing can be straightforward and inexpensive to apply with cesium atoms, as was demonstrated by Watts *et al.* in 1986 [22].

For our thermal beam of cesium, the mean initial velocity along the beam is

expected to be in the neighborhood of $2.3 \times 10^4\,\mathrm{cm/s}$. In chirped-slowing, the peak value of the velocity distribution is not the whole story in determining the optimal chirp range and slowing distance, but it is a good start. Knowing the exact value is not critical for the initial design, and the above value for a typical initial velocity serves sufficiently to design the slower.

The natural lifetime of the $6P_{3/2}$ state sets a practical maximum scattering rate of about 1.6×10^7photons/s, which corresponds to a negative acceleration of $5.7 \times 10^6\,\mathrm{cm/s^2}$. This implies a stopping distance of about 45 cm, which is about the distance of optical access along the cesium beam we had available to slow the atoms before the center of the MOT coils. The initial typical Doppler shift of an atom which can be stopped in 45 cm is 270 MHz, and the slowing sweep would take 4 ms to sweep down to 0 Doppler shift. Experience and the work of Watts *et al.* has taught us that the best slowing occurs when the sweep rate is about 10% less than the theoretical maximum sweep rate. This reduced our estimate of the necessary sweep range to about 235 MHz.

Several methods of producing the well controlled chirp which ends within a few megahertz of a resonance transition have been used by several groups [23][24]. In our research, the $6S_{F=4} \rightarrow 6P_{3/2,F=5}$ resonance is the cycling transition used. Fortunately, the frequency of the master laser, which was already locked to the $6S_{F=4} \rightarrow 6P_{3/2,F=4}$ transition, is 250 MHz lower than the cycling transition. This meant that mixing the slowing laser and the master laser on a beamsplitter and detecting the combined signal on a silicon photodiode would provide a beat-frequency which could be used to heterodyne lock the slowing laser to the master laser. This is the same technique that was used to lock the trapping laser to a fixed offset of the master laser, except that the frequency of the local oscillator for the heterodyne lock is now swept to produce the frequency chirping of the slowing laser.

This method of sweeping the local oscillator has the advantages of being inexpensive and reasonably easy. The photodetector with the necessary 250 MHz bandwidth was constructed with an EG&G FND-100 photodiode and the signal from the photodiode was immediately capacitively coupled to an NE5205 preamplifier for 20dB of

gain. The beat-frequency is turned into an error signal by comparing to a reference frequency signal (i.e., local oscillator) using a circuit based on a Motorola MC4044 phase/frequency detector (figure 2.3). The long period of the linear slowing sweep is well within the range of a simple electronic servosystem that feeds back to the drive current of the laserdiode and to the piezoelectric crystal which moves the orientation of the laser grating.

The heterodyne circuit for the slowing laser is similar to that used for locking our trapping laser relative to the master laser. The primary difference is that while the trapping laser's local oscillator came from an EH1560 programmable pulse generator, the slowing laser lock required a sweeping frequency. This was achieved by feeding an asymmetric triangle wave from a Stanford DS340 arbitrary waveform generator to a voltage-controlled oscillator (VCO), a Texas Instruments 74LS628 IC . Because the laser heterodyne frequency is prescaled down with a divide-by-64, the required range of the VCO is from about 400 kHz up to 3.9 MHz.

Because no acousto-optic or electro-optic elements were placed in the slowing laser beam, all of the laser power was available for slowing. The ending frequency of the sweep was very stable and tunable, which is important for robust and effective cooling, as the ending frequency has the greatest effect on the velocity of the slowed bunches of atoms when they reach the MOT area.

The slowing laser frequency was monitored by deflecting some of the slowing beam with a wedge splitter and producing a saturated absorption spectrum. A good discussion of saturated absorption spectroscopy can be found in Schmidt *et al.* (1994) [25]. When the slowing laser is locked and sweeping correctly, the relevant part of the Doppler free spectrum, including the 4/5 cross-over peak situated 126 MHz below the $6S_{F=4} \rightarrow 6P_{3/2,F=5}$ resonance transition, remains stationary on an oscilloscope synchronized to the voltage sweep going to the VCO. It should be noted that stable locking required the sharp corners on the asymmetric triangle wave to be rounded (low pass filtered) in order to avoid rapid changes the servo could not follow. This is especially important at the corner at the end of the slowing sweep. The chaotic behavior of the servo temporarily losing lock, at this critical time for the slowed atoms,

would otherwise reduce the number of atoms in the MOT loaded from the beam. The rounding was easily accomplished by modifying the programmed waveform of the arbitrary waveform generator with a low-pass filter.

When optimized for the maximum number of atoms in the MOT, the slowing sweep took 4.1 ms and the chirp rate was about 55 MHz / ms as expected. The return sweep took 2.1 ms. Decreasing the return sweep time to less than this caused the lock to come unlocked sooner and did not otherwise noticeably affect the number of atoms in the MOT.

2.3.3 Optical Setup

The optical set up for working with atoms magnetostatically trapped in the $|F = 4, m = 4\rangle$ state is shown in figures 2.4 and 2.5. One change in the optics from our previous experiments with cesium in this state is the use of additional ferroelectric liquid crystals (FLCs). The particular FLCs used were effectively electronically rotatable half-wave plates. They were placed between polarizers and used as reasonably fast shutters. The maximum extinction ratio was about 500 : 1, using cube polarizers and operating at room temperature. This can be improved by another factor of two by using superior polarizers and modifying the temperature of the FLC to take advantage of the small dependence on temperature of the retardation to make the FLC more exactly a half-wave plate. We chose instead to use a second FLC. This requires only one additional polarizer, and allows an intermediate state of transmitted intensity if one of the shutters is open and the other is closed. The FLC shutters take about 30 μs to change state between 10% and 90% transmission. This is significantly slower than using an acousto-optic modulator (AOM) or an electro-optic modulator (EOM) shutter. But the FLC shutter has the desirable properties of having a large clear aperture with little spatial distortion on the transmitted beam, almost 100% transmitted power in the open state, and no alignment sensitivity. In the experiments using atoms magnetostatically trapped in the $|F = 3, m = -3\rangle$ state, a single pass AOM was used. This provided faster switching and a continuously variable

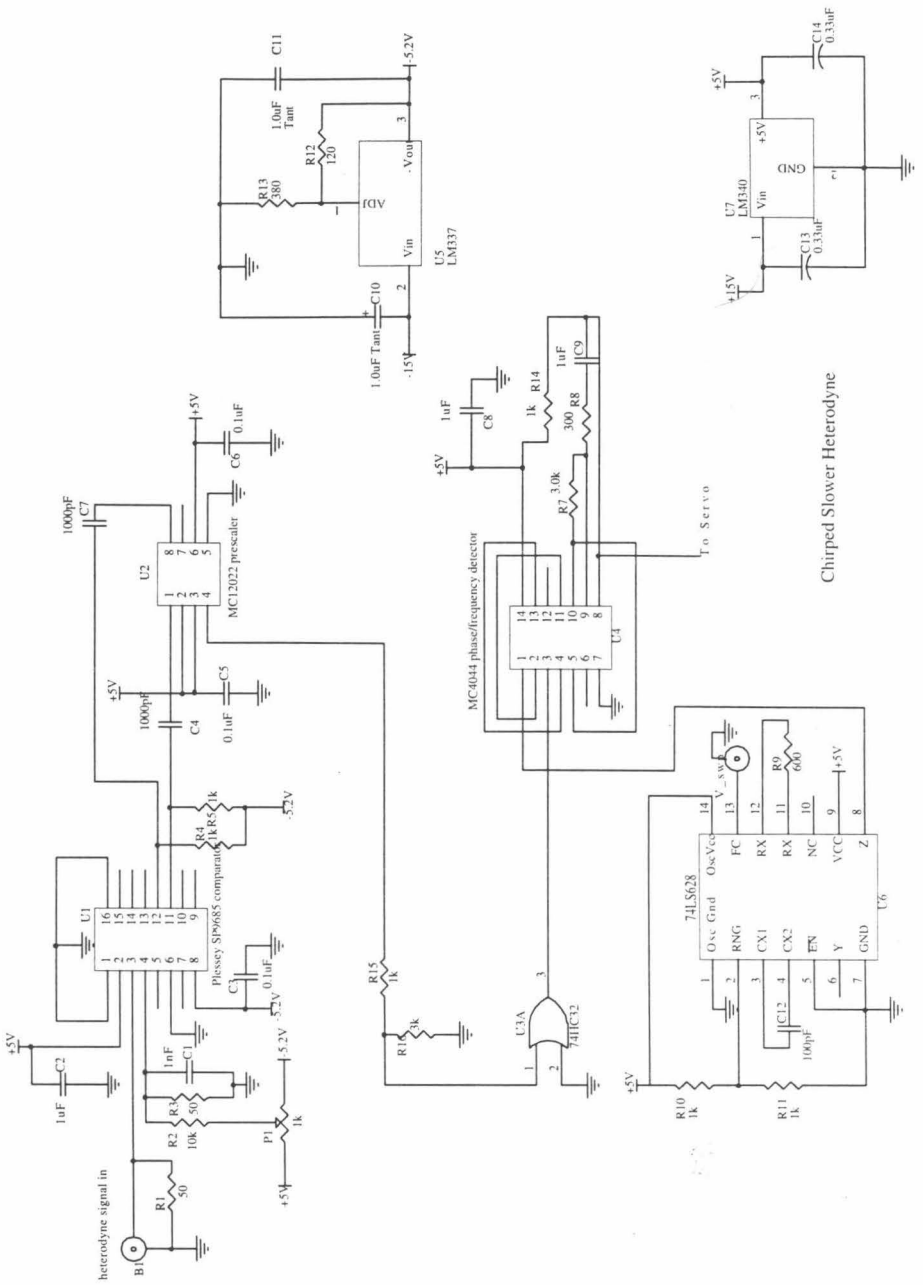

Figure 2.3: The circuit which converts the frequency difference between the externally controllable VCO and the rf signal from the laser heterodyning of the slowing and the master lasers.

transmitted laser power, but FLCs were still used in the repumping beam to begin the exposure for imaging. Two of the FLCs were purchased from Displaytech. The third was purchased from Fabia, an Israeli company, although it is my understanding they no longer offer this product in this form.

The main reason for the increased need for fast shutters in this experiment, compared to previous experiments using the cryotrap, was the change of cameras. The intensified camera used in our previous experiments could be effectively electronically shuttered in nanoseconds by gating the high-voltage to the intensifier tube. The Apogee AP7 slow scan camera could not be electronically gated. Thus the laser beams needed to be turned on after the camera's internal mechanical shutter was known to be fully open, and turned off at the end of the intended exposure time, even though the camera's internal shutter would not close for another 10 ms or so. In order to minimize light leakage, either two consecutive FLCs or a single pass AOM were used in the trapping beam. The repumper did not need an FLC shutter for the experiments with atoms in the $|F = 4, m = 4\rangle$ state, because the atoms could tolerate a few hundred microseconds of this non-resonant light, which allowed the use of a Vincent-Uniblitz fast mechanical shutter. For working with atoms in the $|F = 3, m = -3\rangle$ state, two FLCs were placed in the repumping beam, followed by a slower mechanical shutter.

2.3.4 Imaging Procedure and Atom Number Calibration

A plano-convex lens with a focal length of 34 mm is placed 34 mm from the trap center. A beryllium-copper plate with a one centimeter hole over the lens defines the aperture. The light from the trap is then reimaged on the CCD of the Apogee AP7 slow-scan camera using a commercial compound 50 mm camera lens (figure 2.6). The geometric collection efficiency for this arrangement is thus about $0.067/4\pi = 0.0053 = 0.53\%$. The transmission losses are about 10%, so the total collection efficiency is about 0.48%. The exposure time for the magnetostatic traps was typically about 60 μs, which means every atom has time to scatter roughly one thousand photons, of which

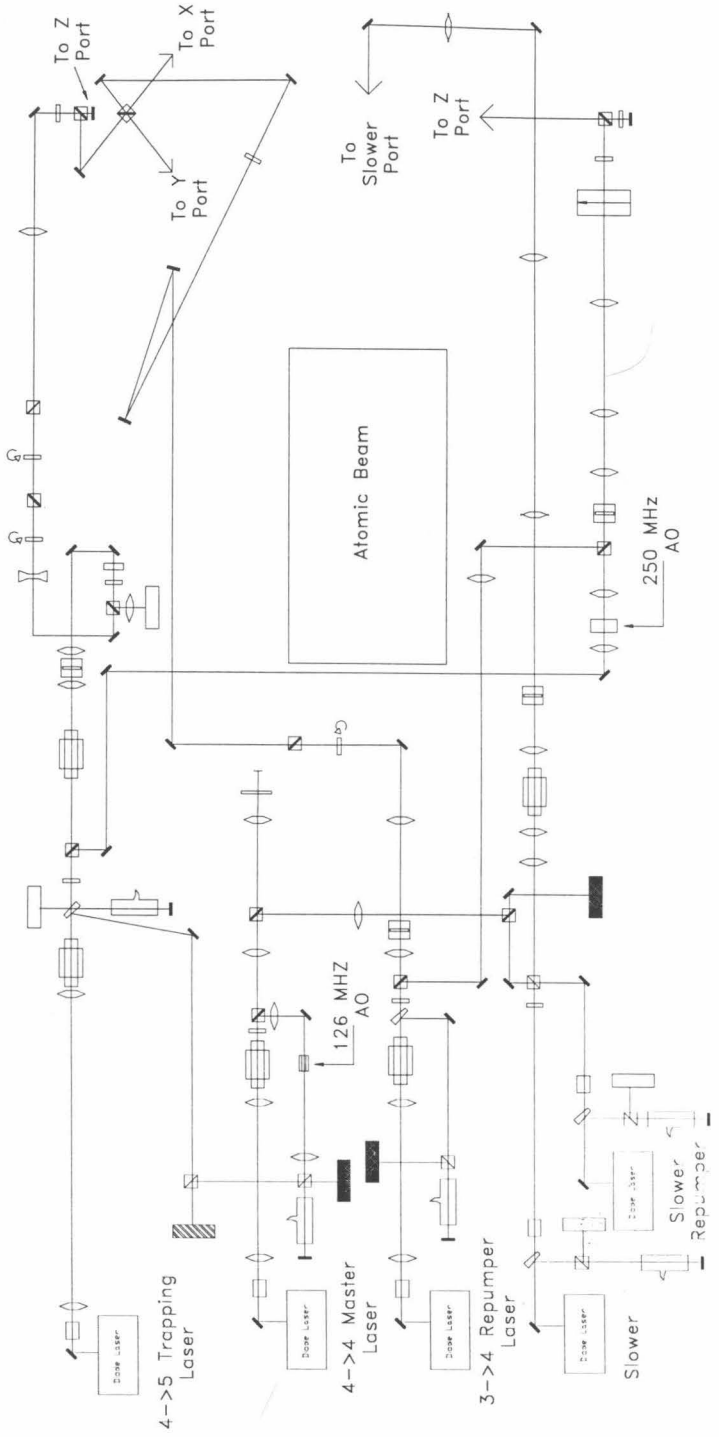

Figure 2.4: The optical system for working with atoms in the F=4, m=4 state in the magnetostatic trap.

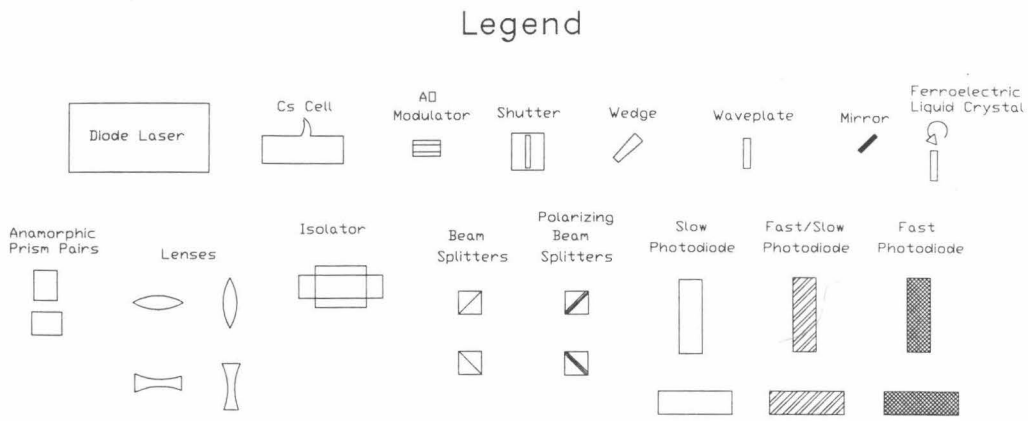

Figure 2.5: Symbols used for optical elements.

about 5 photons per atom will reach the CCD array. The net magnification of the trap image is 2.1 : 1 at the CCD array.

On the opposite side of trap from the lens, light from trap fluorescence is gathered by a 2.54 cm lens of focal length 12.5 cm and collected on a silicon photodiode. Previously, the light collected by the lens internal to the vacuum system had been collected on the photodiode and an external lens had been used for imaging with the Xybion intensified camera, except when performing single atom "images" with the intensified camera. Although the experiments described in this thesis had many atoms, the camera was moved to the position with greater light collection efficiency because the unintensified camera requires more collected light for a given ratio of photon induced signal to the net noise from readout noise and dark current noise. However, the silicon photodiode, which unlike the camera does not have to divide the collected light among thousands of pixels, is more than capable of providing an output with a signal-to-noise ratio of greater than 20 to 1 even though only about 1/20th as much light is collected. The light collection efficiency of the photodiode with the external lens is calculated from the geometric factor to be about 0.029%, and is confirmed by simultaneously measuring the trap fluorescence at the two different

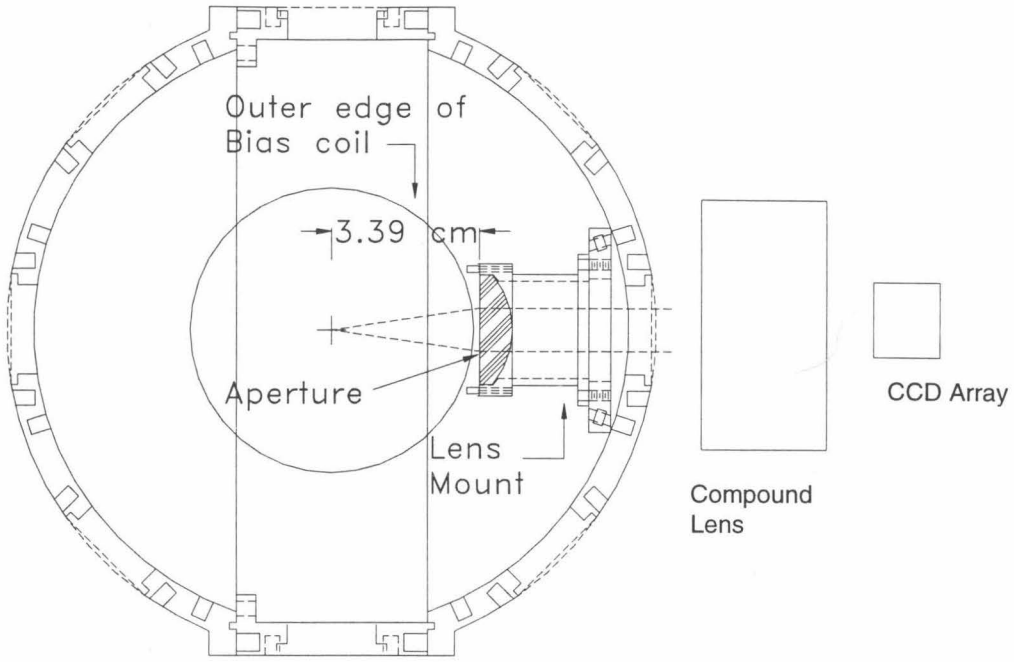

Figure 2.6: The set-up for imaging the trap.

ports, that is, with the internal lens and with the external lens.

The total number of atoms in the MOT and the MST is determined by the fluorescence as measured on the photodiode. This requires a calibration. For a two-level atom with transition rate Γ in a plane wave of Rabi frequency Ω and detuning δ, the power radiated per atom is [26]

$$P_{atom} = \hbar\omega_L \frac{1}{2} \frac{\frac{1}{2}(\Omega^2/\Gamma^2)}{(\delta/\Gamma)^2 + \frac{1}{2}(\Omega^2/\Gamma^2) + \frac{1}{4}}. \tag{2.10}$$

However, a cesium atom in a MOT is far from a simple two level atom. As explained by Townsend *et al.* [27], this expression must be averaged over all the transitions between the Zeeman sublevels in both the ground and excited states. Also, the orientation of the atoms and the local polarization of the laser light is different across the MOT. A method for dealing with these complications, as discussed in a nice review by P. D. Lett *et al.* [6], is to assume that the radiated power can be

expressed as follows:

$$P_{atom} \cong \hbar\omega_L \frac{1}{2} \frac{\frac{1}{2}C_1^2(\Omega_T^2/\Gamma^2)}{(\delta/\Gamma)^2 + \frac{1}{2}C_2^2(\Omega_T^2/\Gamma^2) + \frac{1}{4}}. \tag{2.11}$$

Nominal values of C_1 and C_2 can be found by averaging the Clebsch-Gordan coefficients over all possible transitions. Experimental values can be arrived at by rapidly changing different parameters in different MOTs and observing the change in fluorescence. Townsend *et al.* carried out a careful series of measurements for cesium MOTs and found $C_1^2 = C_2^2 = 0.7 \pm 0.2$.

The effective total Rabi frequency Ω_T is six times the Rabi frequency for any one of the six beams which intersect in at MOT. That is,

$$\Omega_T^2 = 6\Omega^2 = 6\Gamma^2 \frac{I_{avg}}{2I_0}, \tag{2.12}$$

where I_0 is the saturation intensity of the given transition, which for the $F = 4$ to $F' = 5$ cycling transition in cesium is $I_0 = 1.1\,\mathrm{mW}\,/\,\mathrm{cm}^2$, and I_{avg} is the average intensity of each of the six beams.

Determining Ω_T^2 requires a convention for averaging the nonuniform intensity of the laser beams to determine I_{avg}. For Gaussian beams, a common practice is to use, as an effective area, the region contained within the e^{-2} point of the intensity profile. That is, the effective radius of the beam is taken to be the radius at which the intensity of the beam is e^{-2} times the peak intensity, which for a circular Gaussian beam

$$I(r, \phi) = I_0 e^{-r^2/2\sigma^2} \tag{2.13}$$

is simply $r = 2\sigma$. The average beam intensity is then defined to be the total power contained within the e^{-2} radius (about 95% of the total power in the beam for a Gaussian beam), divided by the area, $\pi(2\sigma)^2$.

Experimentally, the intensity profile for our trapping beam was determined by measuring the power transmitted through apertures of various diameters. The mode

Aperture radius (cm)	Fraction of Power Transmitted
0.025	0.005
0.05	0.026
0.1	0.101
0.15	0.220
0.20	0.372
0.25	0.533

Table 2.1: The fraction of the total trapping laser beam power transmitted through circular apertures of various areas

cleaning cavity we used in some previous experiments was not used in this experiment, and without it the beam profile was not well characterized as Gaussian. In particular, if the beam were Gaussian, the fraction of the total power transmitted through an aperture of radius R would be given by the error function, (ratio transmitted) = $\mathrm{erf}(R/\sigma)$. Instead, the transmitted power was seen to increase quadratically with the radius, that is, linearly with the increasing area, as seen in table 2.1 and figure 2.7. This implies that the beam profile, after integrating up the ϕ dependence, is uniform over the range that the transmitted power increases linearly with the area of the aperture. This region includes a disk of radius 0.25 cm, which is about an order of magnitude larger the rms radius of the MOT. And 0.25 cm is also almost twice as large as the e^{-2} radius of the longest magnetostatic traps.

For the purpose of determining the photon scattering rate per atom during imaging of the magnetostatically-trapped atoms, this uniform intensity can be calculated, in terms of the total power, P_{total}, measured for the trapping laser beam to give

$$I_{avg} \cong \frac{1}{3}(2.74)P_{total}\frac{\mathrm{mW}}{\mathrm{cm}^2}, \tag{2.14}$$

where the factor of one-third arises because P_{total} is measured before the trapping laser beam is divided into three beams. There is an estimated 10% optical loss getting the laser to the trap center from where P_{total} is measured, and so a better value for I_{avg} is

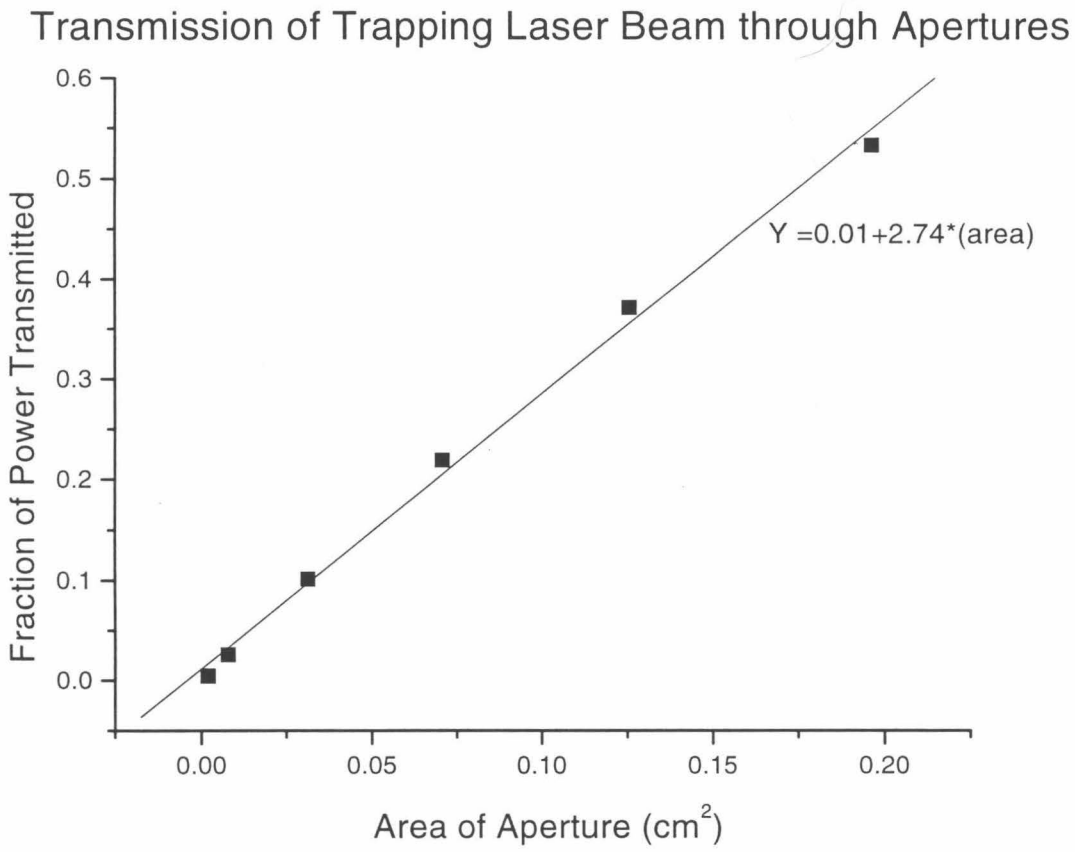

Figure 2.7: The fraction of the total trapping laser beam power transmitted vs. the area of the aperture.

$$I_{avg} \cong \frac{1}{3}(2.5)P_{total}\frac{\mathrm{mW}}{\mathrm{cm}^2}, \tag{2.15}$$

and

$$\Omega_T^2/\Gamma^2 \cong 2.5\frac{P_{total}(\mathrm{mW})}{I_0\ (\mathrm{mW\,cm^{-2}})}. \tag{2.16}$$

This can be used with equation 2.11 to determine the fluorescence per atom. A typical value P_{total} during imaging is 11.5 mW (higher values were sometimes used), for which $\Omega_T^2/\Gamma^2 = 52$. During MST imaging, the detuning δ is chosen to be as small as possible. Even with the external bias field of about 10 G in the MST, $\delta^2 \ll 52$. In other words, the atomic transition is well saturated, and so the dependence of the fluorescence on detuning and intensity is less than linear. This is confirmed by rapidly changing the MOT parameters and watching the fluorescence. For instance, at a trapping laser detuning of $\delta = -1.5\Gamma$, changing P_{total} from 16 mW to 6.5 mW (Ω_T^2/Γ^2 changing from 36 to 15) causes a decrease in MOT fluorescence of only 25%, as predicted by equation 2.11. Together with the calibration of the silicon photodiode and the collection efficiency of the lens, this formula for the fluorescence per atom allows us to determine the number of atoms in the trap to an estimated $\pm 20\%$ accuracy.

2.3.5 Determining the Density and Temperature of Magnetostatically Trapped Atoms

Atoms in a potential $U(\overrightarrow{r})$ will have an equilibrium spatial distribution

$$n(\overrightarrow{r}) = n_0 \exp(-U(\overrightarrow{r})/k_B T), \tag{2.17}$$

where n_0 is the peak density. For the case of a harmonic trap with trap frequencies $\overrightarrow{\omega} = [\omega_x, \omega_y, \omega_z] = 2\pi[\nu_x, \nu_y, \nu_z]$, this becomes

$$n(\overrightarrow{r}) = n_0 e^{-x^2/2\sigma_x^2} e^{-y^2/2\sigma_y^2} e^{-z^2/2\sigma_z^2}, \tag{2.18}$$

where

$$\sigma_x = \frac{k_B T}{m{\omega_x}^2}, \quad \sigma_y = \frac{k_B T}{m{\omega_y}^2}, \quad \sigma_z = \frac{k_B T}{m{\omega_z}^2}. \tag{2.19}$$

The radial symmetry of the trapping potential means $\omega_x = \omega_z$, which implies $\sigma_x = \sigma_y \overset{\text{call}}{=} \sigma_\rho$.

The spatial distribution is the product of three one-dimensional Gaussians. When an image is taken, a column along the camera viewing axis is integrated to produce the two-dimensional image. Fortunately, for this case of a harmonic potential, the distribution is clearly dimensionally separable, and the integration along the, say y, dimension produces a distribution

$$n_{\text{image}}(x, z) = n_0 \sqrt{2\pi}\sigma_y e^{-x^2/2\sigma_x^2} e^{-z^2/2\sigma_z^2}. \tag{2.20}$$

Thus σ_x and σ_z can easily be extracted from the two-dimensional image. When the trap is in equilibrium, the ratio σ_z/σ_x is just $(\omega_z/\omega_x)^2$ and the temperature can be extracted from either σ_z or σ_x, using equation 2.19. In particular, for any dimension i,

$$T = 63\nu_i^2\sigma_i^2\ \mu\text{K}, \tag{2.21}$$

where σ_i is measured in centimeters.

Once either the total number of atoms or the peak density is known, the image of the spatial profile can be used to determine the mean density $\overline{n}$ which is important

in determining the binary collision rate. The definition of $\overline{n}$,

$$\overline{n} = \frac{\int n^2(\mathbf{r}) d^3\mathbf{r}}{\int n(\mathbf{r}) d^3\mathbf{r}}, \tag{2.22}$$

can be immediately evaluated for the case of harmonic potential

$$\overline{n} = n_0/\sqrt{8}. \tag{2.23}$$

Or, using

$$N = \int n(\mathbf{r}) d^3\mathbf{r} = \frac{n_0}{\sqrt{8}\pi^{3/2}\sigma_x\sigma_y\sigma_z} \tag{2.24}$$

we get

$$\overline{n} = \frac{N}{8\pi^{3/2}\sigma_x\sigma_y\sigma_z} = \frac{N}{8\pi^{3/2}\sigma_\rho^2\sigma_z}. \tag{2.25}$$

Thus, we use the total number N as determined from the calibrated photodiode, and σ_ρ, σ_z from the image of the trap, to determine the mean density $\overline{n}$.

Chapter 3 Cross Section Measurements – Theory

3.1 Introduction

If the mean time between elastic collisions for atoms in a magnetostatically trapped sample is much shorter than the lifetime of the trap, elastic collisions between trapped atoms have time to drive the trapped atoms towards thermal equilibrium. This is the case for spin-polarized cesium for the densities, temperatures, and lifetimes in our experiments. If the trap is disequilibrated in a fashion such that the equilibration process can be experimentally observed and understood in terms of the elastic collisions that are driving it, the elastic cross section can be determined. In the next section of this chapter, the theory of elastic-scattering for ultracold spin-polarized cesium is discussed. Following this, the techniques to measure the elastic collision rate by observing equilibration are discussed. In the next chapter the results of our experiments applying some of these methods are presented.

3.2 Ultracold Collisions

For the ultracold cesium atoms of our experiments, the de Broglie wavelength, $\lambda = h/p$, is a few 10s of nanometers, while a typical range for an interatomic potential is about a nanometer [28]. The atoms wave functions will thus overlap during the collision. A quantum mechanical treatment of the collisions is necessary. The way to do this is to expand in partial waves [29]. If k is the relative k for the collision, that is $k = p_{rel}/\hbar$, then the differential cross section is

$$\frac{d\sigma}{d\Omega} = 2\,|f(\theta)|^2 \tag{3.1}$$

when

$$f(\theta) = \frac{1}{k}\sum_{l=0}^{\infty}(2l+1)e^{i\delta_l}\sin(\delta_l)P_l(\cos(\theta)). \tag{3.2}$$

Note that δ_l depends implicitly on k, although it is not always written. The additional factor of 2 is because spin-polarized cesium are identical bosons.

It is conceptually convenient to define

$$f_l \equiv \frac{1}{k}e^{i\delta_l}\sin(\delta_l), \tag{3.3}$$

so that

$$f(\theta) = \sum_{l=0}^{\infty} f_l(2l+1)P_l(\cos(\theta)). \tag{3.4}$$

Then the $\{f_l\}$ contain the k dependence and the information about the interatomic potential. Sometimes the k dependence is made more explicit by writing $f_l(k)$, and other times it is not. Spin-polarized groundstate cesium atoms are identical bosons, and thus only even ($l = 0, 2, ...$) partial wave terms (f_l) are non-zero. Furthermore, for temperatures of a few hundred microkelvin and less, only the first few partial waves are expected to contribute, the higher terms being excluded by the centrifugal barrier. Semiclassically, this can be seen as the situation that for two atoms of such low (relative) speed to have more than a few h of angular momentum, the impact parameter must be outside the effective range of the interatomic force. Much of our experimental results are from samples whose temperatures are $50\,\mu$K and less.

At these temperatures, even $l = 2$ channels are expected to be strongly suppressed. The $l = 0$ channel collisions are called s-wave collisions, and the limit of low energy collisions is thus called the s-wave regime. $P_0(\theta)$ is a constant, so the scattering is uniform in direction. In the s-wave regime, $f_0(k)$ contains all the knowable information about the collision. In particular, if one is only interested in the s-wave scattering cross section, then one only needs to know $|f_0(k)|$. If one takes the limit of $|f_0(k)|$ as $k \to 0$, then one can define the scattering length a as

$$a \equiv \lim_{k \to 0} |f_0(k)| \tag{3.5}$$

$$\lim_{k \to 0} \sigma = 8\pi a^2. \tag{3.6}$$

From equation 3.2, one can see that for s-wave collisions, there exists the so-called unitary limit,

$$\sigma_{0,\max}(k) = 8\pi/k^2, \tag{3.7}$$

where σ_0 stands for the s-wave scattering cross section. The remaining important theoretical result is that the first order expansion for small ak gives

$$\sigma_0(k) = \frac{8\pi a^2}{1 + a^2 k^2}, \tag{3.8}$$

which is immediately seen to be consistent with both the $k \to 0$ limit and the unitary limit.

The average relative momentum between colliding atoms for atoms in a Maxwell-Boltzman distribution is $\langle p_{rel} \rangle = \sqrt{2} \langle p \rangle$, where by equipartition, $\langle p^2 \rangle / 2m = \frac{1}{2} k_B T$, so $\langle k_{rel}^2 \rangle = 2mk_BT/\hbar^2$. Note that the typical k^2 scales as T. Also, note that for a given non-zero temperature, heavier elements will have a larger k^2 and thus a lower unitary limit on their maximum elastic cross section.

If T is low enough such that $a^2k^2 \ll 1$, then σ is nearly $8\pi a^2$ for all collisions. In this case, the collision rate is immediately known from kinetic theory to be

$$\Gamma_{collision} = \overline{n}\sigma_0\overline{v}_{relative} \tag{3.9}$$

where $\overline{n}$ is the mean density, σ_0 is an energy independent cross section, and $\overline{v}_{relative}$ is the mean relative velocity.

The task of calculating the scattering length a for atomic collisions from first principles is increasingly difficult for atoms with higher atomic numbers and nuclear spin. Currently, these calculations have not been accomplished for cesium, the heaviest and most complex stable alkali.

3.3 Techniques for Measuring Ultracold Collision Cross Sections

Prior to the beginning of the work of our group, the only direct measurement of an elastic scattering cross section in spin polarized cesium [30] was for collisions between cesium atoms in the $|3,-3\rangle$ state, the measured value being $(1.5 \pm 0.4) \times 10^{-12}\,\mathrm{cm}^2$. Indirect experimental knowledge of the cesium $|4,4\rangle$ on $|4,4\rangle$ cross section came from the measurements of frequency shifts in a cesium fountain [31] [32], where it was deduced that the $T = 0$ s-wave cross section for this case lay somewhere between $2.5 \times 10^{-11}\,\mathrm{cm}^2$ to $75 \times 10^{-11}\,\mathrm{cm}^2$, which is much larger than the measured value for $|3,-3\rangle$. These fountain experiments also strongly suggested the scattering length a was negative. That is, that the force was attractive, which would allow a bound state at sufficiently low energies and eventually limit the production of higher density, colder, samples. Direct experimental measurements of $|4,4\rangle$ on $|4,4\rangle$ scattering over a range of temperatures were recently published from Laboratoire Kastler Brossel in Paris, France [33]. The first direct measurement of the elastic cross section at a single temperature, $260\,\mu\mathrm{K}$, was previously reported by our group [3], and the temperature

dependence subsequently measured by other groups is confirmed in this thesis.

As previously mentioned, the elastic cross section is measured by preparing the atomic sample in a non-equilibrium (non-thermal) distribution and observing the route to equilibrium, which is driven by elastic collisions. This technique was first employed with ultracold atoms in 1993 [30]. Scattering lengths and cross sections have also been inferred from Bose-Einstein Condensation (BEC) experiments, and the measurements have agreed with the dimensional equilibration method.

A harmonic trap will not couple energy between dimensions, but elastic collisions will. Furthermore, all reported research in magnetostatic traps, including ours, has found that the ergodic timescale for atoms in magnetostatic traps to sample the potential sufficiently such that $(1/2)m\langle v^2\rangle = (1/2)m\omega^2\langle r^2\rangle$ is only a few trap periods, that is, a fraction of a second. Thus, if in the initial distribution of energies in the sample the mean energy in the three dimensions are not equal, observing the rms size of the trap in different directions is an easy way to measure the collision driven approach to equilibrium. The difference between the experiments is primarily the method used to produce this dimensionally non-thermal distribution.

Loading magnetostatic traps produces somewhat non-equilibrium distributions. Purposely mismatching the magnetostatic potential to the initial spatial and velocity distribution can increase this non-equilibrium distribution, and this was the method we used previously to determine the cross section at 260 μK. But this is not a suitable method for the lower temperature measurements, where the energy is close to or below the initial energy of the MOT from which the atoms were loaded. And it is at the lower temperatures where one learns about the important atomic parameter, the scattering length a. At mean energies such that $(ak)^2 \gg 1$, the cross section is dominated by the unitary limit rather than the value of a. Furthermore, because a for cesium was expected to be larger than for any of the other atoms for which it has been calculated or measured, $E \propto k^2$ had to be minimized as much as possible to keep $(ak)^2$ not much greater than 1 in the range a lay.

The method originally used to enhance the dimensional disequilibrium by Monroe *et al.* [30] was parametric heating of one dimension of the trap. The idea here is that

by modulating one or more of the trap spring constants at twice the corresponding frequency, one parametrically drives [34] the atoms and increases their energy in that dimension. Any residual modulation of the spring constants in the other directions does not parametrically drive that dimension as long as the trap frequencies in those directions remain further from the drive frequency than the width of the parametric resonance. This method is efficient at introducing dimensional disequilibrium, but does so at the expense of increasing the total energy of the sample. Another method of producing disequilibrium, which also increased total energy, is a simple technique used by Ketterle *et al.* [36], wherein the center of a linear (gradient) trap was moved non-adiabatically in one dimension, thus adding energy mostly to that dimension.

Much preferred is a method which preferentially cools one or two dimensions of the sample. This has been achieved in several ways. One of the earlier methods, used by Newbury *et al.* [37], employed gravitational Sisyphus cooling [38]. They used it to measure the elastic cross section of ^{87}Rb in the $|F = 1, m_F = -1\rangle$ ground state with a final temperature of $25\,\mu$K at a range of bias magnetic fields. A more common method of cooling samples of magnetostatically-trapped atoms is through evaporative cooling. In particular, the method of rf-induced evaporative cooling, which is discussed in many places, and is summarized with respect to our apparatus elsewhere [3]. The idea of the rf evaporative cooling is to use an oscillating magnetic field to induce spin flips, preferentially in the hotter atoms, which causes those atoms to no longer be weak field seeking and thus not bound by the trap. This reduces the average energy of the remaining atoms. For an Ioffe-type coil set such as ours, rf evaporative cooling is expected to be uniform in all three dimensions, and thus not introduce any dimensional disequilibration. This is in contrast to the TOP trap [39] used by some other groups, in which rf cooling only cools two dimensions. This introduces an inefficiency to overall cooling, but also produces a large dimensional disequilibration, while at the same time reducing the average energy of the atoms. This was very effectively used by Arndt *et al.* in their previously mentioned measurement of the elastic cross section of ^{133}Cs in the $|F = 4, m_F = 4\rangle$ ground state.

For our experiments, we found that even with the Ioffe-type coil set, certain mag-

netic biases and sets of trap frequencies produced very uneven rf evaporative cooling, producing large dimensional disequilibration. As the $|F = 4, m_F = 4\rangle$ ground state is not expected to have any magnetic bias field dependence to the cross section, we used whatever traps produced disequilibration from rf induced evaporative cooling.

In order to associate a measured equilibrium rate with an elastic cross section, one must analyze how collisions drive dimensional equilibration. This has been done with Monte Carlo simulations [30] and by solving the Boltzman equation for somewhat more idealized conditions [43]. Most computer simulations of dimensional equilibration in a harmonic potential assumed a constant cross section. That is, they used the $k \rightarrow 0$ limit for all scattering pairs, which is a reasonable approximation for atomic masses, mean energies, and scattering lengths such that $(ak)^2 \ll 1$. This is a reasonably valid approximation for hydrogen, lithium and sodium because of their relatively small masses, and for cesium in the $|F = 3, m_F = -3\rangle$ state because it has a relatively small scattering length. However, as we shall see in chapter 4, it is a very poor approximation for cesium in the $|F = 4, m_F = 4\rangle$ at all experimentally achieved temperatures. Arndt *et al.* have presented the results of a simulation for the case of a cross section equal to the unitary limit (equation 3.7) at all k, which fit the results of their measurement of the $|F = 4, m_F = 4\rangle$ cross section. In the next chapter, the simulation written to model our experiment will be discussed, and the results will be applied to our experimental data.

Chapter 4 Collision Cross Section – Measurements

4.1 Introduction

The atoms in a magnetostatic trap can be given different mean energies in the axial direction (z-direction) than in the radial directions, and the subsequent dimensional equilibration can be observed. The rate of dimensional equilibration was measured and used to determine the elastic scattering cross section of the atoms, as discussed in the previous chapter. In this chapter, the data obtained using this method is presented, a numerical simulation is presented in order to interpret the data, and the interpretation of the data is presented.

4.2 Experimental Procedure

4.2.1 Loading Atoms into the Magnetostatic Trap

The first step in obtaining magnetostatically trapped and spin polarized atoms is forming a MOT from the slowed cesium beam. The magnetic field gradient for this step was $10\,\mathrm{G}\,/\,\mathrm{cm}$, the laser detuning was $-13\,\mathrm{MHz}$, and the trapping beams were $0.65\,\mathrm{cm}$ in diameter. Without the chirped-slower, and with the cesium beam at $70\,^{\circ}\mathrm{C}$, the MOT contained about 10^6 atoms. With the schirped-slower, the MOT contained about 15 to 20 times more atoms, for a total of about 2×10^7 atoms. A MOT containing as many as 10^7 atoms could be formed without the slower, but at the expense of increasing the cesium beam temperature to $100\,^{\circ}\mathrm{C}$ or higher. However, this greatly increased the background pressure while the beam shutter was open and thus decreased the magnetostatic trap lifetimes. With the cesium beam at $70\,^{\circ}\mathrm{C}$,

the magnetostatic trap lifetime was 100 s – 200 s with the cesium beam shutter open.

For the first set of measurements, the procedure was as follows. A MOT with about 2×10^7 atoms was loaded in a few seconds from the slowed cesium beam. Then a somewhat compressed MOT was formed by increasing the magnetic gradient to 16 G / cm for 25 ms while the trapping laser was further detuned to -18 MHz. The atoms were then cooled somewhat by decreasing the field gradient to 3 G / cm for 3 ms with the trapping laser detuned by -26 MHz and the trapping laser intensity decreased by a factor of 6, such that the intensity was about $2I_{sat}$ in each of the 6 MOT beams. For the $|6S_{1/2}, F = 4\rangle \rightarrow |6P_{3/2}, F' = 5\rangle$ transition, $I_{sat} = 1.1\,\mathrm{mW / cm^2}$.

The trapping beams were then shuttered off, while leaving the repumping beams on, and a σ^+ polarized optical pumping beam aligned along the z-axis and tuned to the $|6S_{1/2}, F = 4\rangle \rightarrow |6P_{3/2}, F' = 4\rangle$ transition was added to drive atoms into the $|6S_{1/2}, F = 4, M = 4\rangle$ state. This optical pumping beam was retroreflected in order to avoid blowing the trap away with unbalanced radiation pressure. The bias field of about 5 G in the z-direction was created with the Bias coil while the atoms were optically pumped for 1.5 ms. All of the lasers were then shuttered off, and the magnetostatic field coils were then turned on. They took about 0.5 s to fully form the magnetostatic trapping potential. For the first set of experiments described below, the atoms were loaded into a trap with frequencies $\vec{\omega} = 2\pi[20, 20, 12.7]$ and bias field $B_0 = 12\,\mathrm{G}$. The currents through the coils necessary to create this magnetostatic potential were $I_1 = 85.5\,\mathrm{mA}$, $I_2 = 224.7\,\mathrm{mA}$, $I_{\mathrm{Bias}} = 95.2\,\mathrm{mA}$, $I_{\mathrm{YY}} = 327.2\,\mathrm{mA}$.

The frequencies of the trap produced by a given set of currents through the coils can be calculated from first principles. But this is not guaranteed to be accurate enough. It is particularly important to have experimental confirmation of the trap frequencies in an experiment such as ours, where the mean energy of the atoms is determined by using the trap frequency and the measured spatial distribution of the atoms in the trap. Any error in the trap frequencies immediately becomes an error in the measured mean energy.

The axial and radial trap frequencies are measured in different ways. The axial trap frequency was measured by two methods. One method was to modulate the

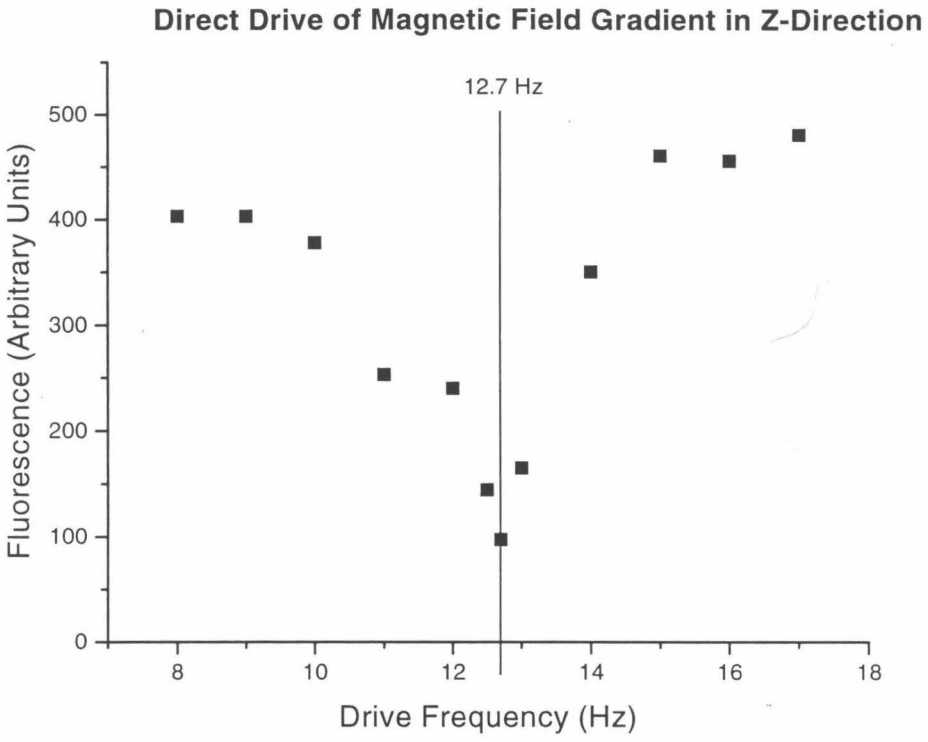

Figure 4.1: Results of direct drive on magnetostatically trapped atoms. The fluoresence is proportional to the number of atoms remaining in the magnetostatic trap after 2 s of drive.

magnetic gradient in the z-direction by about 1 or 2 G / cm at frequencies near the trap axial frequency [35]. This is achieved by applying a sinusoidal modulation of peak-to-peak amplitude 2 mA to the same coils which are used to make the gradient for the MOT. This oscillating gradient causes an oscillating force on the atoms. If the gradient is modulated at a frequency within about ± 0.7 Hz of the axial trap frequency, the atoms quickly leave the trap, as shown in figure 4.1. The frequency at the center of this resonance, 12.7 Hz, is within 6% of 12 Hz, the value calculated from first principles.

The second way to measure the axial spring constant is by changing the magnetic gradient in the z-direction by a known amount and measuring the displacement of

the trap center. This method also allows one to gauge, somewhat, how far from the geometric center the trapping potential remains harmonic on axis. Pushing magnetic gradients, G_z, of $-8.5, -4.25, 4.25$,and $8.5\,\mathrm{G}\,/\,\mathrm{cm}$ were used, and the displacement was seen to agree with $\Delta z = G_z/(2\beta)$ (see equation 2.6), where $v_z = (1/\pi)\sqrt{\mu\beta/2m}$. The agreement with calculation was within a few percent, and is consistent with the systematic measurement error.

The radial trap-frequency was measured by modulating the radial trap frequency. When the modulation frequency is twice the radial trap-frequency, the average kinetic energy of the atoms in the radial dimensions increases. This technique is called parametric drive, and is explained in the previous chapter.

The efficiency rate for optical pumping into the $|F = 4, M = 4\rangle$ groundstate and loading into the magnetostatic trap was $40 - 50\%$. In the magnetostatic trap, the initial mean energy could be as low as $20\,\mu\mathrm{K}\,/k_B$ in all three dimensions, or much more if the MST had large trap frequencies and thus added energy to the atoms during the nonadiabatic formation of the MST. For the trap with $\vec{\omega} = 2\pi[20, 20, 12.7]$, the initial mean energy was about $40\,\mu\mathrm{K}\,/k_B$ with slightly ($\approx 10\%$) higher mean energy in the radial directions than in the axial direction.

4.2.2 Cross Section Measurement and Evaporative Cooling Experiments

The MST was held for three seconds, and then a radio-frequency oscillating magnetic field was applied to the atoms by applying an oscillating current to a small coil mounted inside the cryosphere. The coil has a direct line of sight to the trap center. The coil was not terminated and as such was an unbalanced load. However, below 26 MHz the magnitude of the oscillating field was nearly proportional to a constant times the driving voltage from a $50\,\Omega$ source. The oscillating magnetic field induces transitions between the Zeeman sublevels of the hyperfine state of the trapped atoms, driving them to untrapped states which causes the atoms to leave the trap. Atoms with enough energy to reach magnetic field magnitudes such that the Zeeman split-

ting frequency is close to the frequency of the oscillating field are thus preferentially removed from the trap. This technique is called radio-frequency induced evaporative cooling, and was first carried out with magnetostatically trapped atoms by David Pritchard, as described in a review article [40]. Evaporative cooling of neutral atoms in magnetostatic traps by other means was first proposed [41] and carried out [42] with hydrogen.

For the case of $\vec{\omega} = 2\pi[20, 20, 12.7]$, the radio-frequency cut was at 5.5 MHz and was applied for a second or two. This cut was intended to disequilibrate the trap, and as such removed more atoms than would be necessary for an optimized rf sweep with the same decrease in the mean energy per remaining atom. In particular, for this particular set of coil currents, the rf cooling caused much more cooling in the axial direction than the radial directions, which was followed by re-equilibration, where atoms gained energy in the z-direction and lost energy in the radial directions. We do not know why this particular magnetostatic trap has this dimensionally unequal rf-cut, while most other magnetostatic traps more than incrementally different from this trap have nearly symmetric cooling. Other traps of similar trap frequencies but different magnetic bias (B_0) do not seem to have this unsymmetrical rf-cut, and neither do traps with the same bias field but different trap frequencies. From the perspective of efficient evaporative cooling, this trap is probably merely unfortunate. For collisional equilibration studies, however, the behavior was very fortuitous.

About 50% of the atoms were removed by the rf cut. The mean energies in the three dimensions were measured by imaging the fluorescence from a 50 μs pulse of the trapping laser, which was preceded by a few microseconds by the shuttering on of the repumper laser. In this particular case, the images were very well fit by gaussians, and extracting the root-mean-square position in each dimension was simple. A few seconds after the rf cut, the mean energy was $33\,\mu\mathrm{K}\,/k_B$ in the radial directions and only $19\,\mu\mathrm{K}\,/k_B$ in the axial direction. The measurement technique is quite destructive, and so to determine the time development of the trap the procedure was repeated, waiting between 1 s and 70 s between the rf cut and the destructive measurement. These data are plotted in figure 4.2.

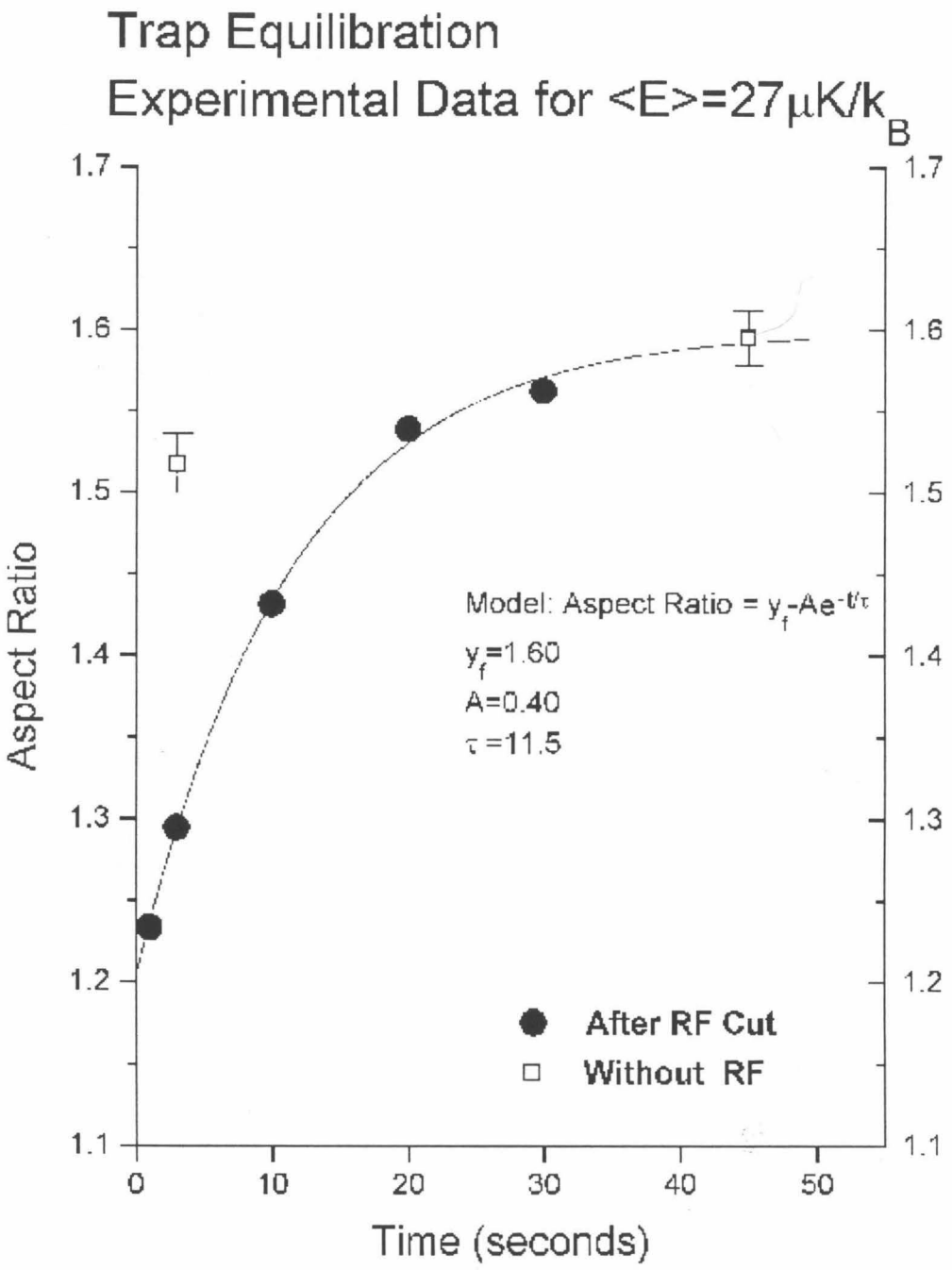

Figure 4.2: The approach to dimensional equilibrium. Each point represents the average of about three points.

Several repeated measurements were taken for each wait time, and the longer and shorter time waits were done in mixed order to help detect any drift in the initial loading conditions of the trap, both in atom number and initial mean energies. By 30 s, the traps had almost completely equilibrated within our experimental ability to distinguish the state from the fully equilibrated state, which was a mean energy of $27\,\mu\mathrm{K}/k_B$ in axial and radial directions. At the longest times, 70 s, the wait time was up to 40% of the trap lifetime, and so there was a significant change in the atom number. Thus on those time scales the collision rate, and the expected equilibration rate, was not independent of time.

The trap loss mechanism is dominated by collisions with much hotter background atoms, and this loss is independent of the energy of the atoms in the trap. That is, the trap loss does not change the mean energy of the atoms in the trap. However, the collision rate has thus changed with time, which would have to be taken into account when extracting the collision rate from the equilibration rate to obtain the cross section. Fortunately, even this was not a major effect, as the longest wait times were only used to determine the asymptotic value of the ratio of the axial and radial rms positions, which was found to agree with the previously measured ratio ω_z/ω_ρ and thus was only a confirmation of the trap frequencies rather than data about the collision cross section of the atoms. Given the known asymptotic value, the relaxation rate could be determined, in simulation and in experiment, with data from times less than or equal to 1/5 of the lifetime of the trap, and the change in atom number during the measured equilibration time was thus less than 20%. This level of trap loss can easily be included in the analysis of the data, and is discussed below in the section on the simulation.

In order to be sure the observed dimensional equilibration was an effect of collisions and not due to cross-dimensional terms in the magnetic potential or other non-collisional effect, the experiment was repeated as closely as possibly with less than one-third the number of atoms, the so called low density case. The initial conditions were not exactly the same, due mostly to the fact that reducing the initial number of atoms in the MOT lowered the initial mean energy per atom. The

frequency of the rf cut then needed to be lowered to have a significant effect on the atoms. Under these conditions the initial dimensional disequilibrium was only about half as large. Nonetheless, the equilibration rate is seen to be about one-third that in the high density case, although the error bars on the rate are larger in this case. The low density case is easier to carry out for the case of parametric heating, where the cause of the disequilibrium is well understood and easier to manipulate to produce a low density case more similar to the high density case. As will be shown below, the equilibration rate decreases proportional to the density in that case, which further confirms that the cross-dimensional equilibration is driven by collisions.

Having succeeded in reducing the average energy per particle and making measurements of the equilibration rate, the next step was to further decrease the average energy of the trap and attempt to make more measurements. One possible method is making deeper (lower frequency) rf cuts with the same trap as for the $27\,\mu\mathrm{K}\,/k_B$ case above. However, removing more than 50% of the atoms in a single cut becomes decreasingly effective at lowering the mean energy with respect to the number of atoms removed. However, if the atoms were instead loaded into a weaker magnetostatic trap before rf-cooling, the initial mean energy would be lower than the previous case of $\vec{\omega} = 2\pi[20, 20, 12.7]$. In particular, we used $\vec{\omega} = 2\pi[13, 13, 8]$. The magnetic bias was $B_0 = 14\,\mathrm{G}$, which is close enough to the previous case to not affect the fluorescence per atom during the measurement.

The initial mean energy of the atoms was, in this case, about $20\,\mu\mathrm{K}\,/k_B$ in each dimension and the initial number of atoms loaded was about the same as in the previous case. This was about the weakest magnetostatic trap which could consistently be loaded from the MOT. The initial size in both measured directions was the same as for the more tightly confining case, suggesting that the latter was adding potential energy to the atoms when the magnetostatic trapping potential was applied. The issue of matching the velocity and spatial distribution of the atoms from the MOT with the trap frequencies of the MST so as to optimize some parameter, such as adding the least energy to the atoms, is a frequent one in magnetostatic trapping experiments. Even if one wishes to decrease the volume the atoms occupy at the expense of increas-

ing their temperature, or decrease their temperature at the expense of increasing the volume, one is better off in both cases loading into the same MST (optimized with respect to the MOT) and adiabatically expanding or compressing the MST. In our case, the $\vec{\omega} = 2\pi[13, 13, 8]$ trap would be considered close to optimized for our initial MOT and optical pumping conditions. After the rf-cut and equilibration, the mean potential energy of the atoms in the trap was about $14\,\mu\mathrm{K}\,/k_B$.

The fluctuations in the both the initial number of atoms and their initial mean energy were larger than in the previous case of the more tightly confining potential, and thus the data is not as clean. A possible reason for the difference is that in the previous case the potential energy gained by the atoms when the MST potential is applied was the dominant effect on the initial mean energy, while in the second case the temperature of the atoms in the MOT and the energy added by optical pumping are the dominant effects. The initial MOT temperature can be effected by the small wandering of the optical trapping beams and small stray magnetic fields in the cryosphere, including those from eddy currents and flux trapping. In contrast, the MST trap harmonic frequencies and the physical center of the potential are very reproducible.

Without a method of cooling one dimension differently than the others below a dimensionally averaged mean potential energy of about $15\,\mu\mathrm{K}\,/k_B$, we were unable to continue investigating lower energy collisions. Instead, we examined higher energy collisions by increasing the average energy of the atoms. Purposefully adding energy to one or more dimensions by increasing the spring constant in that direction or directions can be used for this, as our group did to measure the equilibration rate of atoms with dimensionally averaged mean potential energy $260\,\mu\mathrm{K}\,/k_B$ [3]. This method is inefficient in that it tends to increase the energy in all dimensions, in addition to the desired effect of adding more energy in the radial dimensions than the axial dimension.

A more efficient method of differential heating is parametric drive, which is discussed in the previous chapter. From an experimental point of view, this method has the additional advantage of providing another independent way to measure the

trap frequency.

4.3 Data Analysis and Simulation

We have measured the equilibration rate of trapped cesium atoms in the $S_{F=4,M=4}$ hyperfine state at mean kinetic energies ranging from $14\,\mu\mathrm{K}\,/k_B$ to $260\,\mu\mathrm{K}\,/k_B$. If the elastic cross section is constant over this energy range, then we can easily determine that cross section. The average collision rate, per particle, is [45]

$$\Gamma_{collision} = \overline{n}\sigma_0\overline{v}_{relative} \tag{4.1}$$

where $\overline{n}$ is the mean density, σ_0 is an energy independent cross section, and $\overline{v}_{relative}$ is the mean relative velocity, which for a gas in thermal equilibrium is

$$\overline{v}_{relative} = 4\sqrt{\frac{k_B T}{\pi m}} \approx 1.78\sqrt{T(\mu\mathrm{K})}\frac{\mathrm{cm}}{\mathrm{s}} \text{ (cesium)}. \tag{4.2}$$

It has been shown through simulations [30][47] that for an energy independent cross section and a small enough disequilibration that the collision rate remains nearly constant during the equilibration,

$$\Gamma_{collision} \approx 2.7\Gamma_{eq} = \frac{2.7}{\tau_{eq}}. \tag{4.3}$$

This allows one to immediately extract the cross section from the measured equilibration rate. In that case

$$\sigma_0 \approx \frac{2.7}{\overline{n}\overline{v}_{relative}\tau_{eq}}. \tag{4.4}$$

Where Γ_{eq} is the dimensional equilibration rate of the atoms and $\Gamma_{collision}$ is the collision rate per particle. That is, if N is the total number of atoms in the trap, then $\frac{1}{2}N\Gamma_{collision}$ =(total number of binary collisions per second), as each collision

involves two atoms.

Fitting our data for $27\,\mu\mathrm{K}\,/k_B$ gives $\tau_{eq} = (11.3 \pm 1.5)\,\mathrm{s}$, which would imply $1/\Gamma_{collision} \simeq 4.2\,\mathrm{s}$. For this case, $\overline{v}_{relative} = 9.3\,\mathrm{cm}\,/\,\mathrm{s}$. We find $\overline{n}$ using the calibration discussed in chapter 2 (equation 2.25). In this case, $N \approx 5\times10^6$ and $\overline{n} \approx 3\times10^9/\,\mathrm{cm}^3$. This would imply a measured value of $\sigma_0 \approx 8.4 \times 10^{-12}\,\mathrm{cm}^2$ and $|a| = 5.8 \times 10^{-7}\,\mathrm{cm}$. However, at $27\,\mu\mathrm{K}\,/k_B$, $\overline{k} = 9.7\times10^5\,\mathrm{cm}^{-1}$. This would make $a^2k^2 \approx 0.32$ in equation 3.8. This is beginning to violate the condition $a^2k^2 \ll 1$ required to use the $T \to 0$ limit that $\sigma(k) \approx \sigma_0 = 8\pi a^2$. That is, the magnitude of the scattering length is large enough that the cross section is not independent of k for typical collisions when the mean kinetic energy is $27\,\mu\mathrm{K}\,/k_B$, and so equation 4.3 can not be used to extract the cross section from the measured equilibration rate. However, there is much stronger evidence that the cross section is not energy independent in this range.

That the scattering cross section has an energy dependence is even more readily seen by contrasting $1/(\overline{n}\overline{v}_{relative}\tau_{eq})$ for the $27\,\mu\mathrm{K}\,/k_B$ case above ($3.2\pm0.8\times10^{-12}\,\mathrm{cm}^2$) with the value we measured earlier for the case when the mean kinetic energy was $260\,\mu\mathrm{K}\,/k_B$. In that case [3] $1/(\overline{n}\overline{v}_{relative}\tau_{eq}) \approx (3 \pm 1.5) \times 10^{-13}\,\mathrm{cm}^2$. This factor of about 10 difference is another unmistakable indication that the cross section has a significant energy dependence in this range. A new simulation was necessary in order to correctly interpret our data.

As previously mentioned, Arndt *et al.* have recently also measured the ultracold collision cross section of cesium in the $|F = 4, M = 4\rangle$ state [33]. They report the result of their computer simulation for the case of a resonant cross section, that is, one whose value is the unitary limit (equation 3.7). They follow the lead of Wu and Foot [47] and apply Bird's [49] method of Direct Simulation Monte Carlo (DSMC). I too based my simulation on the DSMC method described by Bird, and on the implementation of the method in his published code. A listing of the main module of the code for my simulation follows in Appendix A.

For a system such as our experiment with $>10^6$ atoms with collisions, the direct simulation of all the trajectories becomes computationally intensive. Even though the mean time between collisions is more than 10 orbits, the overhead for determin-

ing where and when the collisions occur in the simulation is computationally time consuming. A Monte Carlo treatment of the collisions reduces the computation considerably. Bird's method is to separate the trajectory of the atom from the interatomic collisions during small time steps. During each time step Δt_s, every atom is first incremented along its orbit in the external potential. Configuration space is divided into cells whose dimensions are much smaller than the scale of changes in the atomic distribution and much larger than the distance any atom moves during Δt_s. Possible collision pairs are chosen randomly from atoms within the same cell. Whether or not the randomly selected pairs actually collide is determined by an acceptance-rejection method. The probability of acceptance is proportional to the product of the relative velocity and the cross section appropriate for that relative velocity. The post-collision velocities are calculated randomly using an isotropic distribution, as the scattering is almost entirely s-wave for the experimental energy scales.

The number of simulated particles was 10^4 to 10^5, and each simulated particle represented between 20 and 2000 atoms in the range of simulations I carried out. The cell size was between $50\,\mu$m and $100\,\mu$m to a side and the time step was $\Delta t_s = 0.2\,$ms. To test the code, the case of velocity independent cross section was simulated first. The collision rate was found to be nearly independent of time and the relation $\Gamma_{collision} \approx 2.7\Gamma_{eq}$ was reproduced. The collision rate was also found to be $\overline{n}\sigma_0\overline{v}_{relative}$, in agreement with theory.

Next the case of a resonant s-wave cross section, obeying the unitary limit (equation 3.7) was simulated. Because the Δt_s is much less than the timescale on which the average occupation number in a given cell changes, periodic sampling can be used to minimize some of the effects of fluctuations in the cell occupation number, as recommended by Bird. This was tried, but the brute force method of increasing the number of machine particles in the simulation also worked, while also reducing all other observable fluctuations in the output. Without any situation specific methods to reduce fluctuations, 10^4 particles were sufficient to produce the same answers arrived at with simulations using 10 times more machine particles, but with some

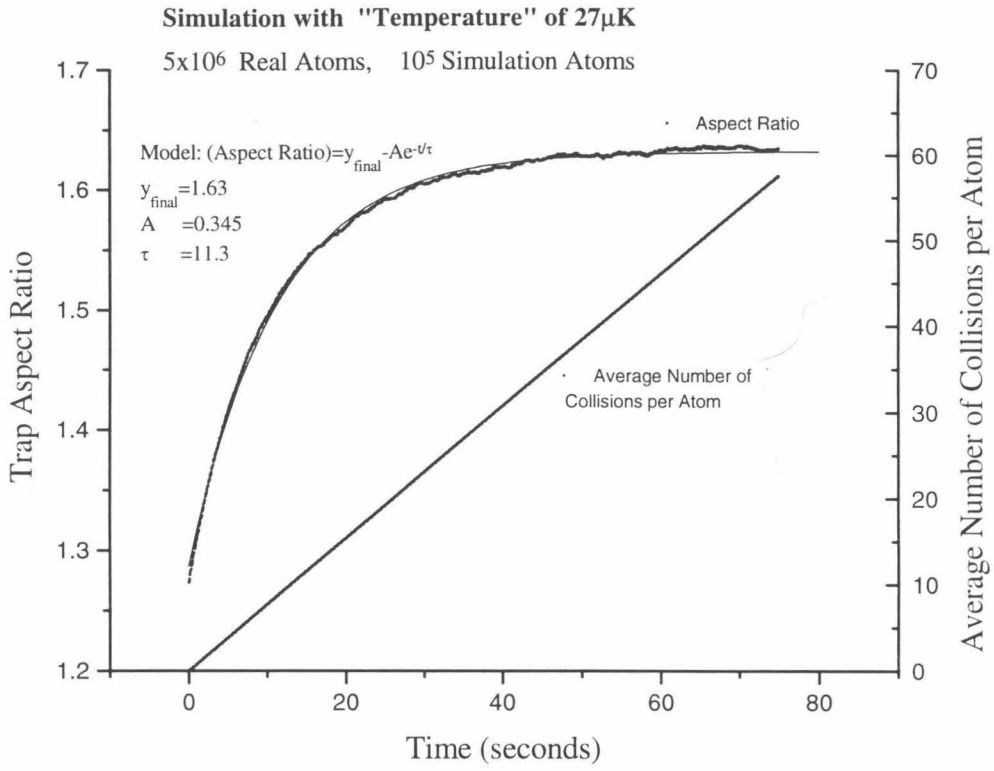

Figure 4.3: The results of a computer simulation using the unitary limit cross-section $\sigma = 8\pi/k^2$. For this simulation, $\tau_{eq} = 8.7/\Gamma_{collision}$.

fluctuations of output variables such as the aspect ratio, in simulated time. Simulations with 5×10^4 or 10^5 particles produced smoother output while still taking only a single overnight computer run on one node of a Sun Enterprise Server. The case most like the experimental parameters of our $27\,\mu\mathrm{K}\,/k_B$ case are shown in figure 4.3.

The initial position and velocity distribution was created by first beginning with Gaussian distributions and then letting the simulation run for about 100 collisions per particle, to be sure the initial pseudorandom distribution represented a machine equilibrium for the algorithm. Whether this initial simulation was performed or not had no discernible effect on the results, and was often abbreviated in later simulations. Next the effect of the rf cut were simulated by scaling the velocities and positions of the atoms as the square root of the ratio of the final and initial mean energy in each

dimension. The rms size in each dimension is later used to determine the ellipticity of the trap as a function of time.

When the atom number is kept constant, the collision rate is constant during the equilibration process. For instance, for the case of figure 4.3, the mean collision rate per particle of 0.77 Hz is constant during the equilibration process, and agrees well with the rate expected for the resonant cross section, $\Gamma_{collision} = 128\overline{n}\hbar^2/\overline{v}^2_{relative}M^2$ [33]. The result from this simulation, $\Gamma_{collision} = 8.7\Gamma_{eq}$, did not vary more than 5% when the number of atoms in the trap simulated was varied in the range 10^5 to 4×10^7.

The measured equilibration rate is thus seen to be in agreement with that expected for a resonant cross section, that is, one limited by the unitary limit $8\pi/k^2$ in the range of interest. As discussed above, the measured value of $1/(\overline{nv}_{relative}\tau_{eq})$ for traps with mean kinetic energy $260\,\mu\mathrm{K}\,/k_B$ is less by about a factor of 10 than that observed for traps with mean kinetic energy $27\,\mu\mathrm{K}\,/k_B$ (figure 4.4). This is the expected signature of a resonant cross section, as k^2 is proportional to kinetic energy. The simulations support the further hypothesis that the proportionality between $\sigma(k^2)$ and $1/k^2$ is 8π as expected. This is in agreement with the published results of Arndt *et al.*, and also provides a correct interpretation for the previously unexplained results at $260\,\mu\mathrm{K}\,/k_B$ reported by our group [3].

4.4 Discussion

The elastic cross section for cesium in the $S_{F=4,m_F=4}$ state for mean kinetic energies in the range $14\,\mu\mathrm{K}\,/k_B$ to $260\,\mu\mathrm{K}\,/k_B$ is seen to be as large as allowed by (non-relativistic) quantum mechanics. At $14\,\mu$K, the elastic cross section is about $5 \times 10^{-11}\,\mathrm{cm}^2$, which is about 8 times the $T = 0$ elastic cross section for sodium [36], 9 times the $T = 0$ elastic cross section for rubidium [37], and 30 times the cross section for cesium in the $S_{F=3,m=-3}$ state [30]. However, we have also seen that the T^{-1} dependence of the cross section on temperature causes the equilibration rate to be about $8.7/2.7 \approx 3$ times less than it would be if the cross section were energy

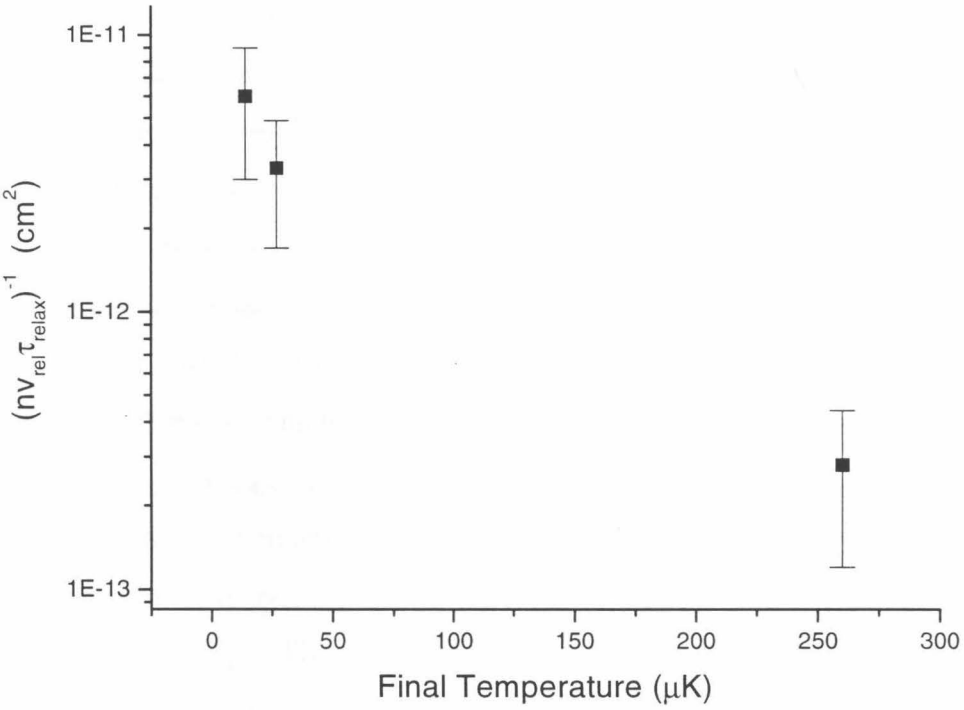

Figure 4.4: The equilibration rate vs. the mean kenetic energy.

independent. The $1/T$ dependence of the resonant cross section also means that adiabatic compression of the magnetostatic trap, which increases the temperature of the atom while increasing their density, is not nearly as beneficial as it is for a light atom, such as sodium, lithium, or hydrogen.

This non-withstanding, the elastic cross section for cesium in the $S_{F=4,m_F=4}$ is large at low temperatures, and continues to increase with further cooling, which increases the net efficiency of evaporative cooling. This made it a good candidate for evaporative cooling. Evaporative cooling in the cryotrap was efficient in all three dimensions, except for the special case we used for measuring the cross section $14\,\mu\mathrm{K}\,/k_B$ and $27\,\mu\mathrm{K}\,/k_B$, and was overall as efficient as expected, up to a point.

The peak density immediately after loading the magnetostatic trap was about $9 \times 10^9 \mathrm{atoms}/\,\mathrm{cm}^3$, and the initial temperature could be made as low as about $20\,\mu\mathrm{K}$. However, we were never able to evaporatively cool a sample below about 7 or $8\,\mu\mathrm{K}$. We were limited somewhat, however, by our inability to accurately measure the temperature of traps with less than a few 10^5 atoms. Söding *et al.* [5] have made a very nice series of measurements of trap loss and heating for evaporatively cooled cesium atoms in the $S_{F=4,m=4}$ state, which show that the inelastic collision rate for cesium is three orders of magnitude larger than for any other previously measured atoms. This giant spin relaxation, as they called it, is a huge hinderance to efficient evaporative cooling. This two body inelastic collision process causes atoms to make hyperfine changing transitions in which one or both of the atoms emerges in the $F = 3$ state, and the difference in the internal energy $\Delta E \simeq h \times 9.2\,\mathrm{GHz}$ per atom that changes hyperfine state is carried away by the atoms as kinetic energy. This energy ($\approx 0.44\,\mathrm{K}\,/k_\mathrm{B}$) is a few hundred times more than the trap depth for the relevant traps, which is a few $\mathrm{m\,K}\,/k_\mathrm{B}$, and so the atoms are lost from the trap. They report an inelastic rate coefficient for this process of $4 \times 10^{-12}\,\mathrm{cm}^3\,/\,\mathrm{s}$. This effectively prevents further efficient evaporative cooling. In particular, BEC of cesium in the $S_{F=4,m=4}$ state is probably impossible.

Chapter 5 A New Cold Slow Atomic Beam

5.1 Introduction

We have designed and constructed a new intense and bright atomic beam source of slow and cold cesium atoms. The design is presented below. Beam intensity is the total flux of atoms divided by the transverse area of the beam. In analogy to optical beams, the intensity divided by the solid angle of the beam divergence is called the brightness. To say the atom beam contains slow atoms means that $\overline{v_L}$, the mean velocity of the atoms along the beam propagation direction, is much smaller than for a so-called thermal atomic beam generated from an oven. Cold refers to the relative smallness of the velocity dispersion of the atoms. In the directions transverse to the atomic beam, cold means that the rms velocity, in those directions, of the atoms is small. In the longitudinal direction, cold means that the root-mean-square, averaged over the atoms in the beam, of the difference between the longitudinal velocity and $\overline{v_L}$ is small.

An intense source of cold slow atoms, which can be turned on and off, is a critical part of many current and planned atomic physics experiments. For instance, for the experiments in the cryotrap, discussed in the previous chapters, the background pressure in the experimental chamber was dominated by the thermal beam and the need, even with the chirped-slower, to allow many atoms into the inner chamber in excess to the slow cesium atoms that were loaded into the trap. A beam slow enough that most of the atoms are collected by the second trap avoids the introduction of untrapped atoms into the lower-pressure chamber. An intense beam can be passed through a narrow opening, which allows much lower pressures to be achieved in the experimental chamber than in the beam source.

Cold atom beams take primarily two forms. The first is slowed thermal beams, where the atoms emerge somewhat collimated from a hot oven and are slowed, and possibly cooled, on their way to their destination. Our chirp-slowed thermal beam is an example of this type.

The second type of intense cold atom beam takes advantage of the powerful concentrating and cooling power of magneto-optical trapping forces to create an atomic source by ejecting atoms form a MOT. Gibble *et al.* [52] showed that atoms can be moved from a MOT to a second trap using a moving optical molasses. Myatt *et al.* [50] developed a so called double-MOT system, where atoms are loaded in a vapor cell MOT which are then transferred, using hexapole magnetic guiding fields and an optical pushing beam, to another MOT in a second cell which had significantly lower background pressure. Both of these techniques are pulsed systems. A technique to make a continuous slow cold atomic beam is an "atomic funnel." The principle behind an atomic funnel is to create a MOT with a leak, so that atoms are fed into a beam as quickly as they can be cooled by a vapor cell MOT. Several atomic funnel type devices have been demonstrated since the first by Riis *et al.* [55]. The most intense of these, and the best suited to differential vacuum techniques which allow a much better vacuum at the terminus of the beam than in initial vapor source of the beam, is the Low-Velocity Intense Source (LVIS) developed by Lu *et al.* [53]. The LVIS is very similar to a normal 6 beam MOT consisting of 3 orthogonal and retroreflected beams, except that one of the retroreflector mirrors has a small (about 1 mm) hole drilled through the center. This creates a column of unbalanced laser light in that dimension through the center of the MOT region. Atoms which enter this region feel a net force towards the hole, and eventually pass through the hole to form the cold and collimated beam. Lu *et al.* have demonstrated that with approximately 4 cm beams, the LVIS is capable of producing an intense beam of rubidium atoms, 5×10^9atoms/s with a longitudinal speed centered at 14 m/s and a FWHM of 2.7 m/s. Their initial beam diameter is about 0.6 mm and the initial divergence is a few degrees, full-angle.

We have designed and constructed a device for producing an atomic funnel, but

which uses a pyramidal mirror system. Forming a magneto-optical trap with one laser beam and a pyramidal configuration of fixed mirrors has been demonstrated by Kim *et al.* [56]. Our system is an attempt to achieve or exceed the performance of the LVIS system with the robustness and simplicity of the pyramid trap. This is motivated partially by the desire to do cold atoms experiments in microgravity environments.

5.2 Design

The concept of the pyramid trap is that instead of the conventional system of mirrors, quarter-wave plates, and beam-splitters required for a 6-beam MOT, one uses a set of four wedge shaped mirrors (i.e., the sides of a pyramid with no bottom) which each make a 90 ° angle with the mirror opposite. The 90 ° reflection the laser beams make upon striking a mirror surface provides the change of circular polarization with respect to the magnetic field necessary to create counter-propagating σ_+ and σ_- beams as required for a MOT.

A pyramid tapers to a point, and this is the natural place to extract atoms from the MOT for a beam. We achieve this by truncating the wedge-shaped mirrors, topping the resulting truncated pyramid with a gold-coated quarter-wave plate as was used in the LVIS beam. A back-coated quarter-wave plate, instead of simply a mirror, is necessary to make the reflected beam have the correct circular polarization for magneto-optical trapping. A 1 mm diameter hole was laser drilled in this wave plate, and it is through this hole the beam is to be extracted. In order to extract the atoms out of the trapping region, the mirrors must be placed inside the vacuum system. The vacuum chamber is cylindrical (figure 5.5), and so the mirrors are rounded on top to almost meet the wall of the vacuum chamber. A drawing of the mirror used for each side of the pyramid is shown in figure 5.1.

Gold coated glass mirrors were chosen for the sides of the pyramid, primarily for their high optical quality. These mirrors are supported by an aluminium support which holds all four mirrors and also holds the drilled and coated quarter-wave plate.

This monolithic structure, which I will call the central piece, insures the relative orientation and position of the separate optical components in the vacuum chamber, and effectively defines the center line of the optical system. The center piece does not extend the full length of the mirror. Additional support is provided for each mirror by an aluminum bracket (figure 5.2) upon which the backs of the mirrors rest. The center piece is shown in cross section, with the brackets, in figure 5.3, and from the top and bottom (without the brackets) in figure 5.4. To permanently fix the alignment of the mirrors, and to allow the system to be tilted on its side, the mirrors are stuck to the central piece and to the brackets with a two-part, high-vacuum-compatible epoxy. The epoxy is sold under many brand names, the most common of which is probably Torr-Seal, which is sold by Varian Vacuum Products. The drilled and coated quarter-wave plate rests in a small depression as seen in the drawing, and is held in place by short pieces of beryllium-copper which are screwed into the central piece.

The entire assembly of the central piece, the supporting brackets, and the mirrors which are attached to them, is attached by screws to a 10 in to 2.75 in zero-length adapter. This adapter attaches to one of the 10 in flanges of the vacuum system and has a 2 in diameter hole through which the atoms are extracted. On the other side of the adapter, a 14 in long square-profile glass tube is attached. Eventually, when this atomic beam is used as a beam source for other experiments, the 1 mm hole in the quarter-wave plate will provide an excellent low conduction interface between the beams vacuum chamber and the future experiment's vacuum chamber. In the molecular-flow region, the conductance of an aperture for a gas of molecular weight M is [57]

$$C = 3.7A\sqrt{\frac{T}{M}}, \tag{5.1}$$

where M is the molecular weight (133 for stable cesium), A is the area of the aperture in area in cm^2, and T is the temperature in Kelvin. The conductance of the 1 mm

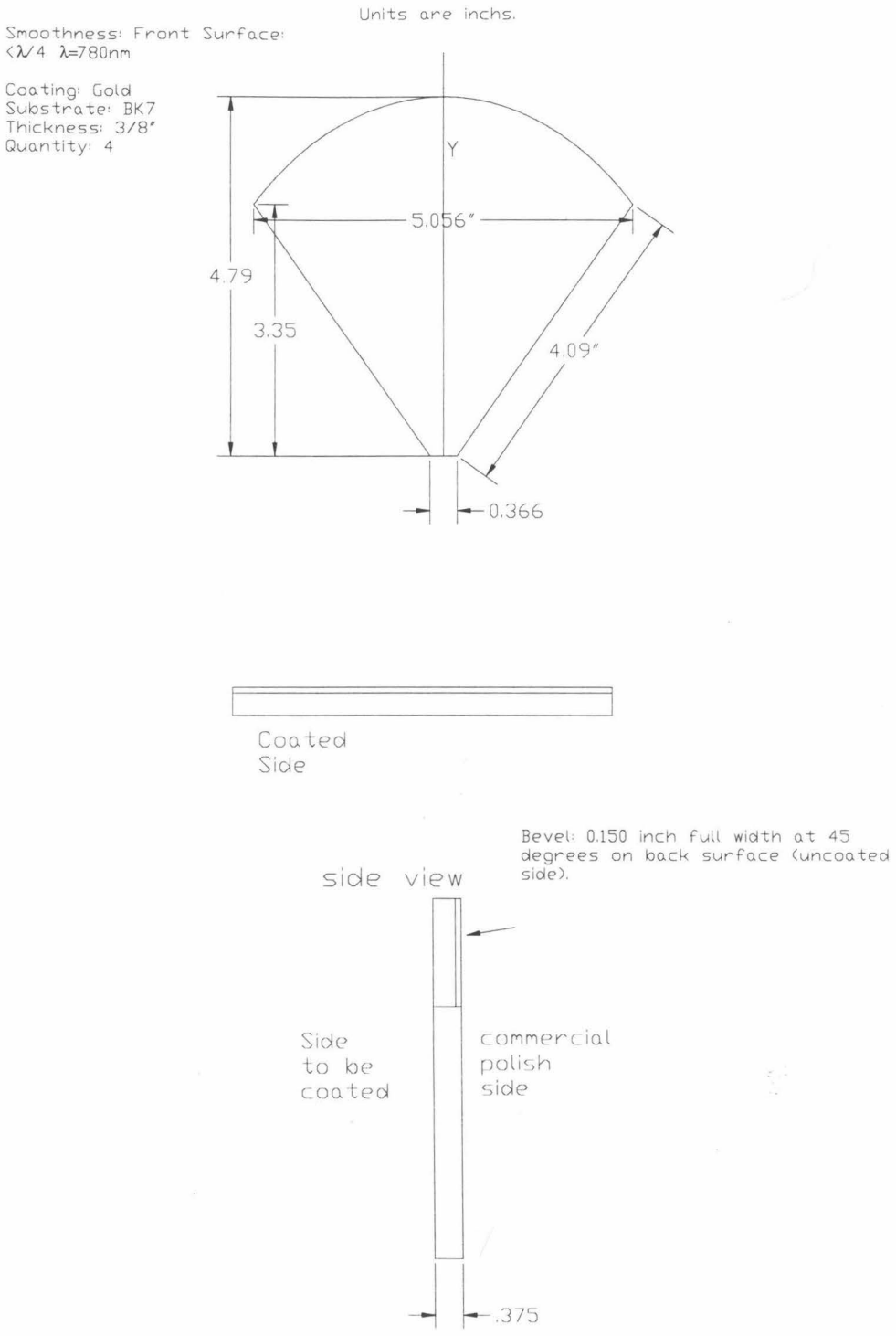

Figure 5.1: The mirrors for the pyramid trap.

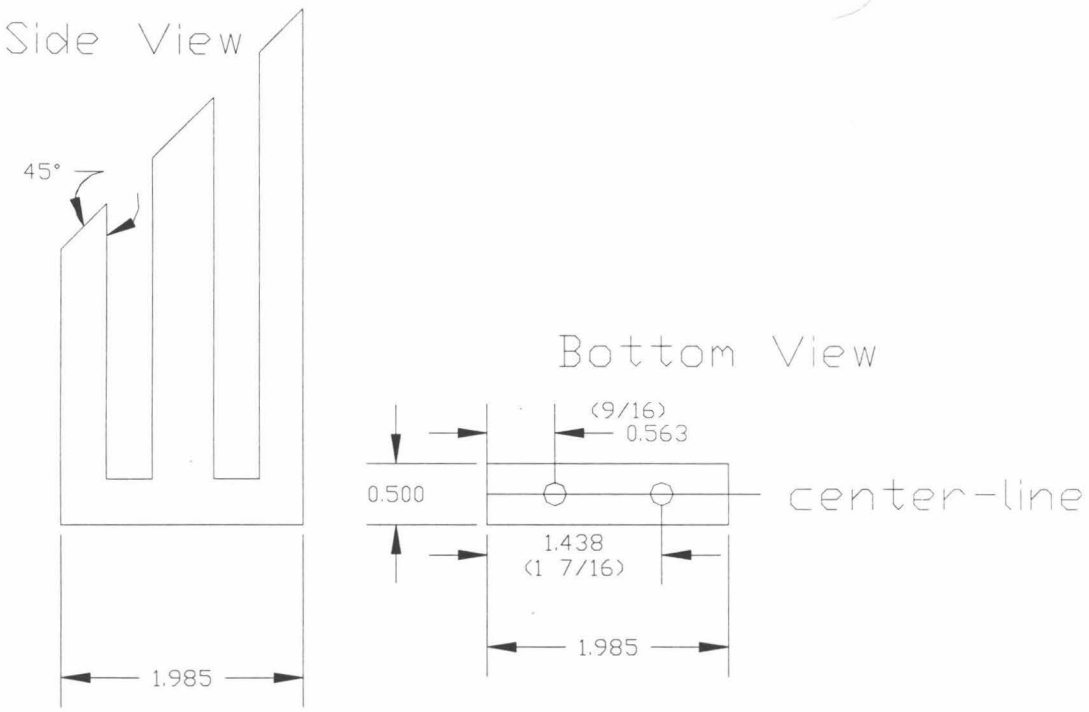

Figure 5.2: The side bracket. One of these per mirror is used to support the part of the pyramid mirrors not supported by the central piece.

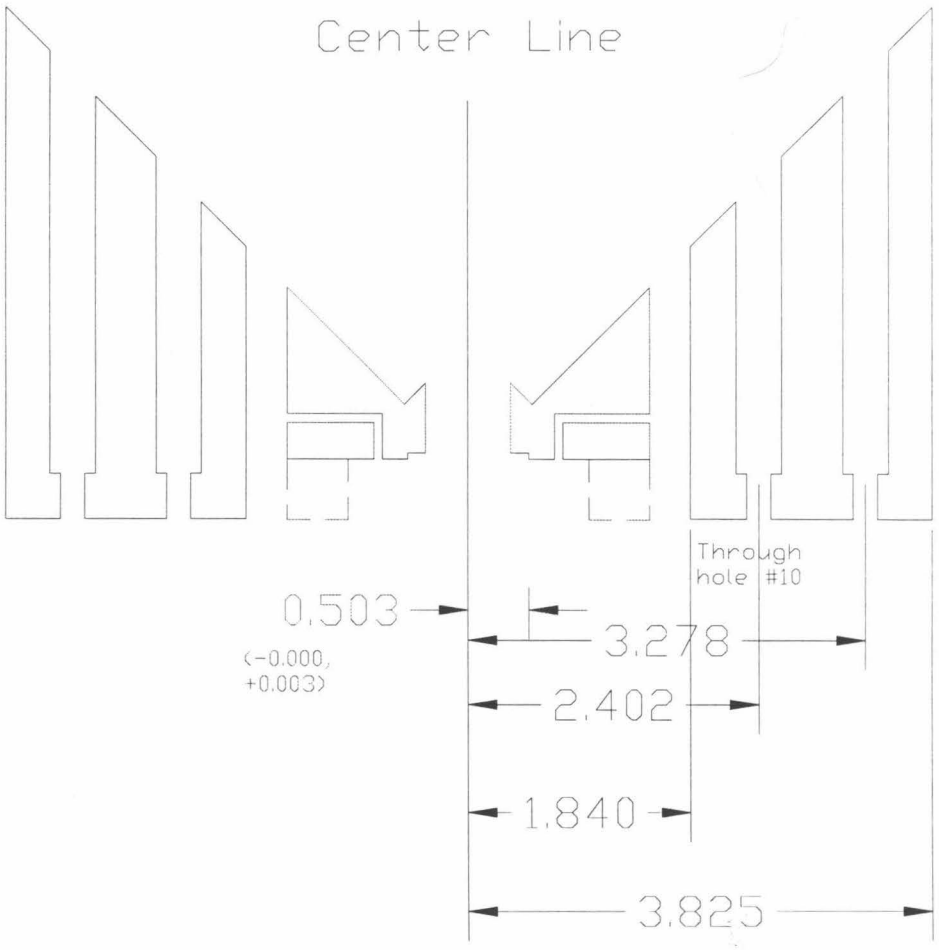

Figure 5.3: Cross section of the brackets for holding the mirrors. The central piece and two of the side brackets are visible. Objects behind the cross section are either not shown or shown with dashed lines.

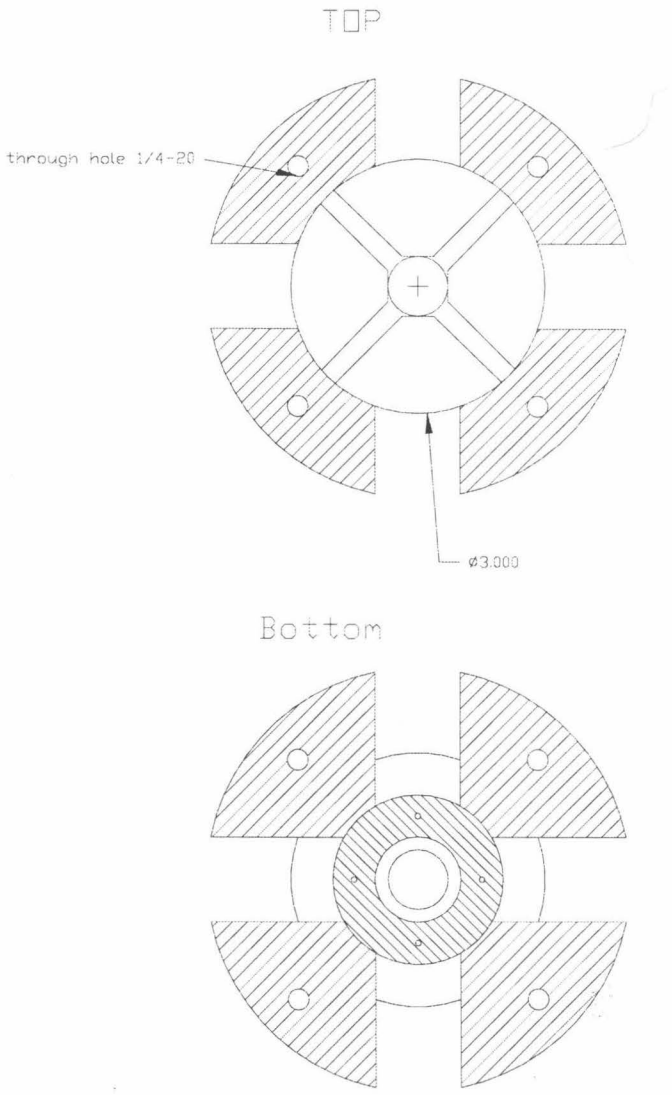

Figure 5.4: The central piece for holding the 4 pyramid mirrors and the coated quarter-wave plate.

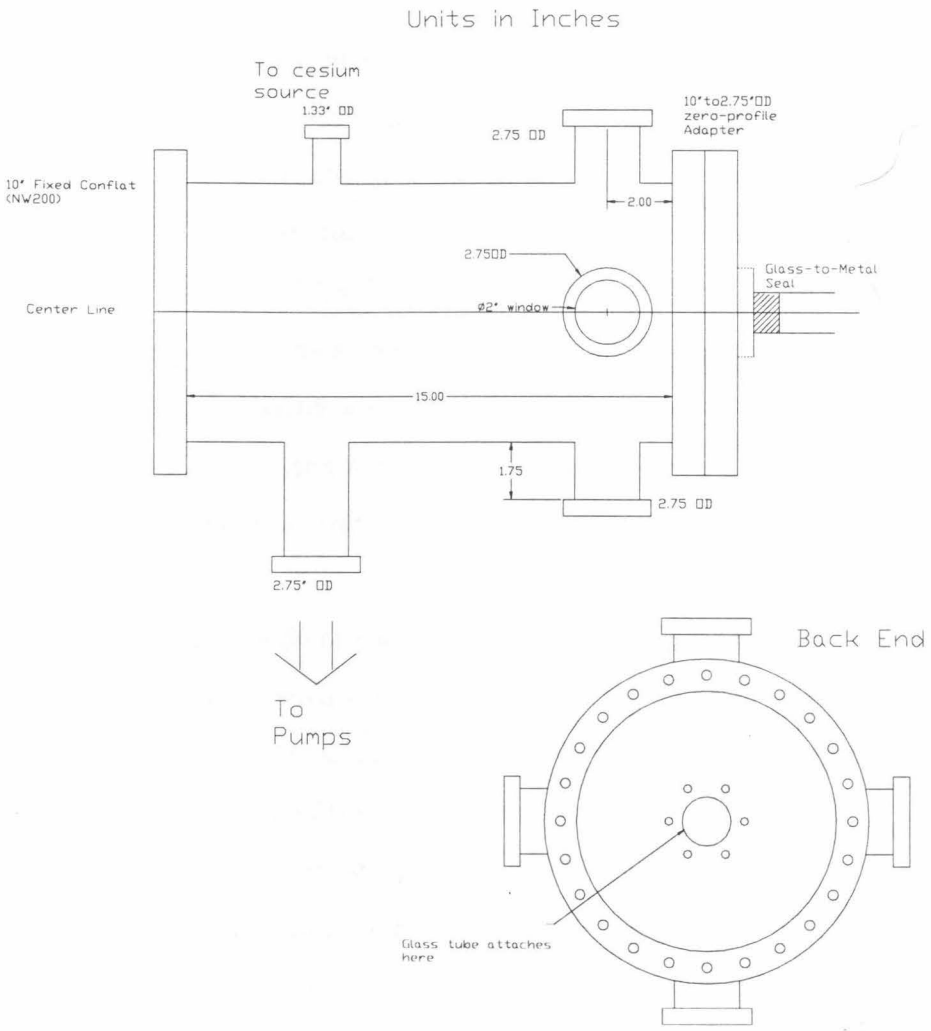

Figure 5.5: Schematic drawing of the vacuum chamber.

diameter hole for cesium would then be only about $0.05\,\mathrm{l\,s^{-1}}$. The conductance for hydrogen would be about $0.5\,\mathrm{l\,s^{-1}}$ and for helium about $0.25\,\mathrm{l\,s^{-1}}$, but the background partial pressure of hydrogen and helium are both an order of magnitude less than the cesium pressure. Thus their rate of flow through the aperture is at worst equal to the flow of cesium. The heavier elements, other than the cesium which is purposely loaded into the chamber, are expected to be less abundant in the background gas than hydrogen and helium, and will have a lower conductance than hydrogen and helium as well. This low molecular flow of background atoms out of the beam source should allow a pump on the far side of the aperture to achieve very low background pressures. For instance, an ideal $50\,\mathrm{l\,s^{-1}}$ pump on the far side of the aperture would be able to achieve 100 to 1000 times less background pressure than the pressure in the beam source, while still having access to an intense source of cold and slow atoms. For the purposes of this experiment, however, the glass cell did not have an independent pump, but rather was evacuated by means of additional holes to the main beam source.

On the opposite side of the vacuum chamber from the pyramid mirrors, the other 10 in flange is sealed with a vacuum window which has a 7.75 in clear diameter (the inner diameter of the vacuum chamber), and which has been anti-reflection coated for 780 nm and 852 nm, the D_2 lines of rubidium and cesium respectively. The laser beam needs to be expanded almost up to the full 7.75 in of the vacuum chamber to fully take advantage of the available mirror area, although smaller beams are acceptable and could even prove desirable for certain applications. In order to create a laser beam up to 7.75 in in diameter, a beam expander was implemented using both a conventional glass lens for the first element and a commercially available 10 in diameter, focal length of 60 in, gold coated parabolic mirror for the second element. The initial beam size is one or two tenths of an inch, and so the first lens needs a focal length of about one inch. In order to not block the expanded beam, the incoming beam to the 10 in mirror has to be off-axis. However, the outside of the input window's flange is only 5 in from the center of the input beam, so the incoming beam need only be about $5\,\mathrm{in}/60\,\mathrm{in} \approx 80\,\mathrm{mrad} \approx 5\,^\circ$ off-axis. This is not seen to significantly affect the

outgoing collimated and enlarged beam.

The magnetic field gradient required to form a magneto-optical trap is produced by a set of coils that fit over the long dimension of the vacuum chamber. Their inner radius, R, is about 18 cm and each coil has 320 turns of 12 gauge magnet wire. The diameter of this wire is about 2.05 mm which means a resistance per length at room temperature of about $0.0051\,\Omega\,/\,\mathrm{m}$. The final wire resistance is about $2.1\,\Omega$ per coil. With the coils separated by $R = 18\,\mathrm{cm}$ for the maximum gradient at given current, the coils together produce about $1.2\,\mathrm{G}\,/(\mathrm{cm\,A})$. With 5 A through each coil, the coils get a little warm, while at 10 A they get rather hot. The optimal field gradient is expected to be less than or equal to about $6\,\mathrm{G}\,/\,\mathrm{cm}$, so the heating should not be a problem.

5.3 Operation

The chamber was transported to Jet Propulsion Laboratory (JPL), Time and Frequency Standards Division, where the 500 mW to 1 W of tunable stable laser power was to be provided. The vacuum was roughed out with a turbo-pump, and then a $12\mathrm{l\,s^{-1}}$ ion pump was engaged. After a day or two, the pressure in the chamber was about 1.5×10^{-8} torr. At this point a glass ampule, containing 1 g of cesium, inside a thin-walled steel tube attached to the main chamber by a manifold, was crushed, releasing the cesium. In order to drive the cesium through the manifold connecting the steel tube to the main chamber, the steel tube and the entire manifold was heated to about 100 °C for several days, with occasionally heating to 150 °C. The pressure in the chamber was monitored by retroreflecting a near resonant laser probe beam around the pyramid and back out of the chamber, and measuring the absorption of this probe compared to the absorption through a cell which is only about 1/10 as long but which contains a partial pressure cesium of a few 10^{-6} torr. After a few days of heating the cesium and the manifold, the partial pressure of cesium in the main chamber could be adjusted between about 10^{-8} torr and a few 10^{-7} torr within about 10 minutes by adjusting the temperature of the cesium source.

Unfortunately, recent and continuing laser stability troubles at JPL have prevented actually testing the atomic beam. A more stable, Ti:Sapphire, laser on the optical table with the atomic beam has recently become available and the staff members at JPL hope to test the atomic source in the next 2 to 5 weeks.

If the beam source is functional when tested, future plans for its application include sympathetic cooling and polarization of ions in one of the ion traps at JPL or changing the beam to working with rubidium and loading traps for a Bose-Einstein Condensation experiment.

Appendix A The Monte Carlo Simulation

```
#include<math.h>
#include<stdio.h>
#include"sim1.h" /*Defines some numerical constants*/
/*******  Information about Cell and Subcell Structure ***/
/* NCX is number of cells in x dimension (etc).
#define NCX 39
#define NCY 39
#define NCZ 39
#define NC  (NCX*NCY*NCZ)
/***** nscx is # of sub-cells per cell, in x dim*/
#define NSCX 1
#define NSCY 1
#define NSCZ 2
/* Characterize Initial Atom Distribution */
#define MASS (2.206e-22)     /*Mass of CESIUM(133) in grams*/
/************** Global Variables************************/
/**Variables to Keep track of certain events*********/
int totSelected=0, totOort=0,vreltoosmall=0,totgone=0;
long unsigned int SELT=0;  /*Total Number of Pair Selections */
long unsigned int totalSteps=0;/*Total # of timesteps taken*/
long unsigned int NCOL=0; /* Total # of Collisions */
/****** Cell structure variables***/
int NSC = NC*NSCX*NSCY*NSCZ; /*Total Num of all SubCells */
double cwx=0,cwy=0,cwz=0,cvol=0;
/* cwx is cell width, cwy is cell height, cwz is depth*/
/* in units of cm.  cvol is the volume(cm^3) of each cell*/
/* Geometry Factors */
double cgxmin[NC]; /*low x border of cell*/
double cgxmax[NC]; /*high x border of cells */
double cgymin[NC]; /* etc... */
double cgymax[NC];
double cgzmin[NC];
double cgzmax[NC];
int *IP; /*IP[i] is subcell atom i is in*/
/******** Some Parameters and default values. Runtime Values
determined by values read from file param.in  ***/
/* # real atoms rep. by each computer particle */
int NUMSIM = 100;
double DT= 0.0002;  /*timestep in seconds  */
/****Variables used to calculate cross-sections*******/
double gTref =1.0;  /*in microkelvin (effects kBoltz) */
double SREF= 7.2e-10; /*Ref X-section at gTref, in cm^2*/
unsigned int NUMINIT=10000; /*Num. of machine particles */
/* Information about MST trap parameters */
float W[3];   /* trap frequencies in 3-dim (radian/sec)*/
int *oort; /* Keeps track of status of each atom */
/*OutOfRangeTrajectory:1=OutOfBins, 0=In Bins, -1=Left Trap*/
```

```
/****Passing RANSEED around makes the psuedorandom
number generation reproducable.  ********/
/* Any function using ran1 should have RANSEED*/
long int RANSEED=-21155; /*Default value */
void main(void) {
  /*indexCell[i] is the position in indexR for atoms in cell**/
  unsigned int indexCell[NC];
  unsigned int numinCell[NC]; /*Number of Atoms in Cell*/
  unsigned int isc[NSC]; /*Cell that subcell is in*/
  unsigned int indexSubCell[NSC]; /*Index info for subcells*/
  unsigned int numinSubCell[NSC]; /*Number of atoms in subcell */
/*** indexR is an ordered list of the atoms, in increasing order of
   which cell they are in.  So (if cell zero has at least one atom)
   indexR[0] is the particle number of an atom in cell zero, and
   indexR[1] is another particle in cell zero, or an a particle in
   cell one if cell 0 has only 1 atom ***/
  unsigned int *indexR;
  int *gone; /* atoms that were at some time out of all cells */
  float ccg[NC];   /*Est. Max. value (X-section)*(v_rel) in Cell*/
  float ccgRem[NC]; /*Remainder when selection number is rounded*/
  FILE *datafile, *fin, *fout,*frestart=NULL,*fplot;
  char s[80],s2[80];/*Temp. string variables*/
  int initxsc[NSC],initxc[NC];
  /*Matrices of particle positions and velocities */
  float **pp, **pv;
  /** Variables for loops for sampling and file writing **/
  int fileWrites=0,totalFileWrites=0,
    samplesPerFileWrite=0,samples=0;
  int timestep=0,stepsPerSample=0,resetNCOL=0;
  double stepsPerFileWrite; /*Just used for output*/
  int i,j,k,m,i2,m2,tempint,totpart,centercell;
/***Variables used only for initial distribution*/
  /* T[i] is 'temperature' for ith-dim*/
  double T[3];/*Used Only for creating initial dist*/
/* pmp is PositionMostProbable[x y z]
           (i.e. mean absolute value of position)*/
  double pmp[3];
  double vmp[3]; /*Speed Most Probable[x y z] */
/*Temp variables, used within a few lines of assignment*/
  double tempdouble,tempdouble2,tempdb,tempdb2;
  float tempfloat,tempfloat1,tempfloat2,rem,A;
/*Variables used for keeping track of total and
           average values over all atoms*/
  double KE,PE,v2[3],d2[3],v[3],d[3];
  float pixelspercm=880;
/****** End of variable declerations*********/
/****** Set trap frequencies ***/
  W[0]= (2*PI*20.5);
  W[1]= (2*PI*20.5);
  W[2]= (2*PI*12.7);
/******Initialize some arrays */
  for(i=0;i<NC;i++)  {
    indexCell[i]=0;
    numinCell[i]=0;
```

```
    initxc[i]=0;
  }
  for(i=0;i<NSC;i++) {
    isc[i]=0;
    indexSubCell[i]=0;
    numinSubCell[i]=0;
    initxsc[i]=0;
  }
/**** Load some parameters from input file */
  if( (fin=fopen("param.in","rt"))==NULL) {
    printf("Couldn't Open data.in for reading.  Aborting\n");
    exit(-2);
  }
  fgets(s,80,fin);
  sscanf(s,"%ld",&RANSEED);
  printf("From param.in RANSEED=%ld\n",RANSEED);
  if(RANSEED>0)
    RANSEED=-RANSEED;
  if (RANSEED==0){
    printf("0 Initial RANSEED. QUITTING\n");
    exit(-3);
  }
  fgets(s,80,fin);
  sscanf(s,"%d %s",&stepsPerSample,s2);
  printf("%d :: %s\n",stepsPerSample,s);
  fgets(s,80,fin);
  sscanf(s,"%d:: %s",&samplesPerFileWrite,s2);
  printf("%d :: %s\n",samplesPerFileWrite,s);
  fgets(s,80,fin);
  sscanf(s,"%d %s",&totalFileWrites,s2);
  printf("totalFileWrites=%d :: %s\n",totalFileWrites,s);
  fgets(s,80,fin);
  sscanf(s,"%d %s",&NUMINIT,s2);
  printf("NUMINIT=%d :: %s\n",NUMINIT,s);
  fgets(s,80,fin);
  sscanf(s,"%d %s",&NUMSIM,s2);
  printf("NUMSIM=%d :: %s\n",NUMSIM,s);
  fgets(s,80,fin);
  sscanf(s,"%d %s",&resetNCOL,s2);
  printf("Reset NCOL=%d :: %s\n",resetNCOL,s);
  fclose(fin);
/**** Setup output files ********/
  if( (fout=fopen("data.out","wt"))==NULL) {
    printf("Couldn't Open data.out for writing.  Aborting\n");
    exit(-2);
  }
  if( (fplot=fopen("plot.dat","wt"))==NULL) {
    printf("Couldn't Open plot.dat for writing.  Aborting\n");
    exit(-2);
  }
/***** Initialize random number generator */
  ran1(&RANSEED);
  printf("after initialization, ranseed=%ld\n",RANSEED);
  /*Initialize Variables */
  T[0]=40.0; /* Temp is in microKelvin */
  T[1]=40.0;
```

```
  T[2]=40.0;
  /*Cell Dimensions (each cell, in cm) */
  cwx=cwy=0.009;
  cwz=.016;
  cvol=cwx*cwy*cwz;
  /*Define origin at center of trap */
  cgxmin[0]=-cwx*((float)NCX)/2.0;
  cgymin[0]=-cwy*((float)NCY)/2.0;
  cgzmin[0]=-cwz*((float)NCZ)/2.0;
  centercell=NCX*NCY*(NCZ-1)/2+NCX*(NCY-1)/2+(NCX-1)/2;
  /* Assign Cell Edge coordinates */
  for(i=0;i<NCZ;i++) {
    for(j=0;j<NCY;j++) {
      for(k=0;k<NCX;k++) {
      /*Set X-coords of Cell */
        if(!k)
          cgxmin[m]=cgxmin[0]; /*Left edge of a Leftmost cell*/
        else
          cgxmin[m]=cgxmax[m-1];/*Use Right edge of previous cell*/
        cgxmax[m]=cgxmin[m]+cwx;
     /*Set Y-coords of Cell */
        if(!j) /*First y-line (at this z)->Least y-value*/
          cgymin[m]=cgymin[0];
        else if(!k) /* Not 1st, but still new y-line */
          cgymin[m]=cgymax[m-1];
        else /* Just another x increment, leave ymin alone */
          cgymin[m]=cgymin[m-1];
        cgymax[m]=cgymin[m]+cwy;
     /*Set Z-coords of Cell */
        if(!i) /*First z-line*/
          cgzmin[m]=cgzmin[0];
        else if (!j && !k) /*New z-line (not first),
                             incr. zmin to old zmax*/
          cgzmin[m]=cgzmax[m-1];
        else /*Just another cell, no change in zmin */
          cgzmin[m]=cgzmin[m-1];
        cgzmax[m]=cgzmin[m]+cwz;
/* Set initial (estimated) max[(sigma)(v_rel)] in each cell */
/* sigma in cm^2 and v_rel is in cm/sec */
        ccgRem[m]=ran1(&RANSEED);
        ccg[m]=(30.0*SREF)/(T[0]+T[1]+T[2]);
      }
    }
  }
  /*Set sub-cells */
  for(i2=0;i2<NC;i2++){
    for(i=0;i<NSCZ;i++){
      for(j=0;j<NSCY;j++) {
        for(k=0;k<NSCX;k++) {
          m=i2*NSCX*NSCY*NSCZ + i*NSCX*NSCY + j*NSCX + k;
          isc[m]=i2; /*subcell m is in cell i2 */
        }
      }
    }
  }
  do {
```

```
    printf("Start new or continue (n or c)? :");
    scanf("%s",s);
    printf("\n");
  }while(s[0]!='c' && s[0]!='C' && s[0]!='n' && s[0]!='N');
 /*If new simulation, generate initial dist*/
  if (s[0]=='n' || s[0]=='N') {
    /*Find most probable speeds and displacements */
    for(i=0;i<3;i++) {
      vmp[i]=sqrt(2.0*KBOLTZ*T[i]/MASS);
      pmp[i]=vmp[i]/W[i];
    }
    printf("vmp=[%g %g %g]\n",vmp[0],vmp[1],vmp[2]);
    printf("pmp[0]=%g  pmp[2]=%g\n",pmp[0],pmp[2]);
    /* Allocate some matrices and arrays*/
    pp=newfloatmatrix(NUMINIT+1,3);
    pv=newfloatmatrix(NUMINIT+1,3);
    IP=newintarray(NUMINIT);  /*Subcell atom is in */
    oort=newintarray(NUMINIT);
    indexR=newunsignedintarray(NUMINIT);
    gone=newintarray(NUMINIT);
    for(i=0;i<NUMINIT;i++) {
      /* Assign initial coords. and subcells */
      do {
        for(j=0;j<3;j++)
          pp[i][j]=ranvel(&tempdouble,&tempdouble2,pmp[j]);
        tempint=assignSubCell(pp[i]);
        if (tempint<0)
/* negative sign means out of range for assignSubCell */
          printf("Atom %d was trying to be oort, disregarded.\n",i);
      }while(tempint<0);
      oort[i]=0;
      gone[i]=0;
      indexR[i]=0;
      IP[i]=tempint;
      initxsc[tempint]++;
      initxc[isc[tempint]]++;
    }
    fileWrites=0;
    tempint=0;
    for(i=0;i<NC;i++)  {
      tempint+=initxc[i];
    }
    fflush(fout);
    /***Assign atom velocities, independent of positions***/
    tempdb=tempdb2=0;
    for(i=0;i<NUMINIT;i++) {
      for(j=0;j<3;j++)  {
        pv[i][j]=ranvel(&tempdouble,&tempdouble2,vmp[j]);
        tempdb2+=SQR(pv[i][j]);
        tempdb+=SQR(pp[i][j]*W[j]);
      }
    }
    printf("%d atoms: PE=%g  total 'ke'=%g\n",NUMINIT,tempdb,tempdb2);
  }/* End of "if new" */
  else{ /*Read from restart file */
```

```
    printf("Reading from restart file\n");
    if( (frestart=fopen("restart.dat","rb"))==NULL) {
      printf("Couldn't Open restart.dat for reading.  Aborting\n");
      exit(-2);
    }
    fread(&RANSEED,sizeof(long int),1,frestart);
    printf("RANSEED=%ld\n",RANSEED);
    fread(&fileWrites,sizeof(int),1,frestart);
    printf("fileWrites=%d\n",fileWrites);
    fread(&NUMINIT,sizeof(unsigned int),1,frestart);
    printf("NUMINIT=%u\n",NUMINIT);
    printf("Param.in: real per simulated particle is :%d\n",NUMSIM);
    /* Allocate some matrices and arrays*/
    pp=newfloatmatrix(NUMINIT+1,3);
    pv=newfloatmatrix(NUMINIT+1,3);
    IP=newintarray(NUMINIT);  /*Subcell atom is in */
    oort=newintarray(NUMINIT);
    indexR=newunsignedintarray(NUMINIT);
    gone=newintarray(NUMINIT);
    for (i=0;i<NUMINIT;i++)
/* read stored velocities from file*/
      fread(pv[i],sizeof(float),3,frestart);
  for (i=0;i<NUMINIT;i++)
/* read stored  positions from file*/
      fread(pp[i],sizeof(float),3,frestart);
    fgets(s,80,frestart);
    sscanf(s,"%lu",&NCOL);
    printf("NCOL=%lu\n",NCOL);
      NCOL=0;
    }
    for(i=0;i<NUMINIT;i++) {
      indexR[i]=0;
      gone[i]=0;
      oort[i]=0;
      tempint=assignSubCell(pp[i]);
      IP[i]=tempint;
      initxsc[tempint]++;
      initxc[isc[tempint]]++;
    }
  }/*End of use restart file*/
  stepsPerFileWrite=
      (double)samplesPerFileWrite*(double)stepsPerSample;
  index3(pp,pv,numinCell,indexCell,numinSubCell,indexSubCell,
      indexR,isc,gone);
/*** The principal loops of the simulation **/
  for(;fileWrites<totalFileWrites;fileWrites++){
  /** Initialize some variables used for running sums*/
    totpart=0;
    for(i=0;i<3;i++){
      v2[i]=0;;
      d2[i]=0;
    }
    PE=0;
    KE=0;
    for(samples=0;samples<samplesPerFileWrite;samples++) {
```

```
  for(timestep=0;timestep<stepsPerSample;timestep++) {
    move3(pp,pv,isc,gone);
   totalSteps++;
   index3(pp,pv,numinCell,indexCell,numinSubCell,indexSubCell,
      indexR,isc,gone);
   coll3(pp,pv,ccg,ccgRem,numinCell,indexCell,numinSubCell,
    indexSubCell,indexR,isc);
  }/*(end of loop: timestep) */
  for(i=0;i<NUMINIT;i++) {
   if(oort[i]==0) {
    for(j=0;j<3;j++)  {
       tempdouble=SQR(pv[i][j]);
      v2[j]+=tempdouble;
       KE+=tempdouble;
      tempdouble=SQR(pp[i][j]);
       d2[j]+=tempdouble;
      PE+=tempdouble*SQR(W[j]);
    }
     totpart++;
  }
  }
  printf("Samples=%d  fileWrites=%d\n",samples,fileWrites);
  /** Open Next data file **/
  sprintf(s,"data%d",fileWrites);
  strcat(s,".out");
  printf("s=%s\n",s);
  if( (fout=fopen(s,"wt"))==NULL) {
    printf("Couldn't Open %s (data) to write. Abort.\n",s);
    exit(-4);
  }
  printf("Avg Total PE=%g, KE=%g\n",
      PE/stepsPerFileWrite,KE/stepsPerFileWrite)
  printf("Center Cell (#%d) has %d atoms\n",
      centercell,numinCell[centercell]);
/** Write next data file **/
  printf("fileWrites=%d Steps=%lu  total Time=%g\n",
fileWrites,totalSteps, (float)totalSteps*DT);
  fprintf(fout,"fileWrites=%d Steps=%lu  total Time=%g\n",
  fileWrites,totalSteps,(float)totalSteps*DT);
  printf("Total: PE=%g  KE=%g totpart%u\n",
  PE/stepsPerFileWrite,KE/stepsPerFileWrite,totpart);
  fprintf(fout,"Total: PE=%g  KE=%g totpart=%u\n",
  PE/stepsPerFileWrite,KE/stepsPerFileWrite,totpart);
  printf("currently totOort=%d\n",totOort);
  fprintf(fout,"rms v :%g %g %g\n",sqrt(v2[0]/totpart),
    sqrt(v2[1]/totpart),sqrt(v2[2]/totpart));
  fprintf(fout,"rms poss :%g %g %g\n",sqrt(d2[0]/totpart),
sqrt(d2[1]/totpart),sqrt(d2[2]/totpart));
  fprintf(fout,"rms poss :%g %g %g\n",
    pixelspercm*sqrt(d2[0]/totpart),
    pixelspercm*sqrt(d2[1]/totpart),
    pixelspercm*sqrt(d2[2]/totpart));
  printf("rms v :%g %g %g\n",sqrt(v2[0]/totpart),
  sqrt(v2[1]/totpart),sqrt(v2[2]/totpart));
  printf("rms pos (cm) :%g %g %g\n",sqrt(d2[0]/totpart),
```

```
      sqrt(d2[1]/totpart),sqrt(d2[2]/totpart));
      printf("rms poss (pixels) :%g %g %g\n",
        pixelspercm*sqrt(d2[0]/totpart),
      pixelspercm*sqrt(d2[1]/totpart),
        pixelspercm*sqrt(d2[2]/totpart));
      fprintf(fout,"%lu #Computer Collisions\n",NCOL);
      fprintf(fout,"%lu #Real Collisions\n",NCOL*NUMSIM);
      fprintf(fout,"%lu #totalSteps\n",totalSteps);
      fclose(fout);
    /**** Write Restart File ****/
      if(frestart!=NULL)
        fclose(frestart);
      if( (frestart=fopen("restart.dat","wb"))==NULL) {
      printf("Couldn't Open restart.dat for writing.  Aborting\n");
      exit(-2);
    }
    fwrite(&RANSEED,sizeof(long int),1,frestart);
    printf("2: Ranseed=%ld\n",RANSEED);
    fwrite(&fileWrites,sizeof(int),1,frestart);
    fwrite(&NUMINIT,sizeof(unsigned int),1,frestart);
    /* The array is broken up into NUMINT seperate fwrites because
some compilers (eg. linux gcc up through at least 2.7.1) screw up
when using fwrite with large blocks.  For example, linux
gcc 2.6.3 fwrite will mess up if passed more than about 77Kb
at once */
    /* Store current velocities*/
    for(i=0;i<NUMINIT;i++)
    fwrite(pv[i],sizeof(float),3,frestart);
    /* Store current positions */
    for(i=0;i<NUMINIT;i++)
      fwrite(pp[i],sizeof(float),3,frestart);
    printf("Total Sim Collisions:%lu => %lu collisions\n",
      NCOL,NCOL*NUMSIM);
    printf("Steps=%lu  totOort=%d\n",totalSteps,totOort);
    fprintf(frestart,"%lu     #Computer Collisions\n",NCOL);
    fclose(frestart);
    tempfloat1=(sqrt(d2[0]/totpart)+sqrt(d2[1]/totpart))/2.0;
    tempfloat2=sqrt(d2[2]/totpart);
    /*** Write plot file ***/
    fprintf(fplot,"%g  %g  %g %g\n",2.0*(float)NCOL/(float)NUMINIT,
    tempfloat1,tempfloat2,tempfloat2/tempfloat1);
    fflush(fplot);
  }/* (end of loop: fileWrites) */
  fclose(fplot);
}
/*********** Function coll3 *****************************/
/**** Calculate collisions of atoms *********************/
int coll3(float **pp, float **pv, float *ccg, float *ccgRem,
  unsigned int *numinCell, unsigned int *indexCell,
  unsigned int *numinSubCell, unsigned int *indexSubCell,
  unsigned int *indexR,unsigned int *isc) {
  int cn,intsel,isel,i,avn;
  unsigned int atom1,atom2;
  float numsel; /*numsel is the num. of pairs to be selected*/
  float speedrel,vrel2,cvr,cvm,tempfloat;
```

```
for(cn=0;cn<NC;cn++) {
  /* Can use current numinCell times a time averaged one
  like Byrd does, but it made no visible difference for
  my simulation*/
  numsel=0.5*SQR((float)numinCell[cn])*(float)NUMSIM*
      ccg[cn]*DT/cvol;
  /* numsel is expected number of collisions to take
  place in this cell */
  numsel += ccgRem[cn];/*Add the remained from previous*/
  intsel=(int)floor(numsel);/*Can only carry out integer
                              number of collisions*/
  ccgRem[cn]=( numsel-floor(numsel));/*Store fraction part*/
  if(numinCell[cn]>1 && intsel>0)/*If cell has 2 atoms to collide*/
  totSelected+=intsel; /*Total number of collision pairs */
  cvm=ccg[cn]; /*ccg[cn] is "max sigma_v*v_rel" in cell*/
  for(isel=0;isel<intsel;isel++) { /*Do Collisions */
/* Given first atom, psuedorandomly chose a near one for collision*/
    selectp(cn,&atom1,&atom2, numinCell,indexCell,numinSubCell,
        indexSubCell,indexR,isc);
/*Calculate relative v and v^2 of these two atoms */
    tempfloat=0;
     for(i=0;i<3;i++) {
      tempfloat+=(SQR(pv[atom1][i])+SQR(pv[atom2][i]));
    }
    vrel2=0;
    for(i=0;i<3;i++) {
      vrel2+=SQR(pv[atom1][i]-pv[atom2][i]);
    }
    speedrel=sqrt(vrel2);
    if (vrel2<0.00001) {
      printf("Collision pair rejected, vrel2 too small\n");
      vreltoosmall++;
        printf("vreltoosmall=%d\n",vreltoosmall);
    }
    else {
    /* X-section goes as 1/k^2, Unitary Limit*/
      cvr=speedrel*32.0*(PI*HBAR2/SQR(MASS))/vrel2;
    /* constant value resonant logic */
        /*cvr=speedrel*(Insert constant X-section here);*/
      if(cvr>cvm)
        cvm=cvr;
  /* Apply acceptance-rejection */
      tempfloat=ran1(&RANSEED);
      if(tempfloat < cvr/ccg[cn]) {
     /* Then accept collision *//
        NCOL++; /* Keep track of total number of collisions */
        elastic(atom1,atom2,pp,pv,speedrel);
        tempfloat=0;
        for(i=0;i<3;i++)
        tempfloat+=(SQR(pv[atom1][i])+SQR(pv[atom2][i]));
        ccg[cn]=cvm;
      }
    }
    }
  }
}
```

```
}
/************ Function elastic() ***************************/
int elastic(unsigned int atom1, unsigned int atom2, float **pp,
            float **pv, float speedrel) {
  float a,b,c;
  /*vrelpc is 1/2 the post-collision relative vel. */
  static float vrelpc[3];
  static float velcm[3]; /*The velocity of the center-of-mass */
  int i;
  for(i=0;i<3;i++)
    velcm[i]=0.5*(pv[atom1][i]+pv[atom2][i]);
  b=2*ran1(&RANSEED)-1.0;
  /* b is the cosine of a random elevation angle */
  a=sqrt(1.0-b*b);
  vrelpc[0]=0.5*b*speedrel;
  c=2.0*PI*ran1(&RANSEED);
  /*c is the random azimuth angle */
  vrelpc[1]=0.5*a*cos(c)*speedrel;
  vrelpc[2]=0.5*a*sin(c)*speedrel;
  for(i=0;i<3;i++) {
    pv[atom1][i]=velcm[i]+vrelpc[i];
    pv[atom2][i]=velcm[i]-vrelpc[i];
  }
}
/************* Function selectp() ***********************/
  int selectp(int cn,unsigned int *a1,unsigned int *a2,
  unsigned int *numinCell, unsigned int *indexCell,
  unsigned int *numinSubCell, unsigned int *indexSubCell,
unsigned int *indexR, unsigned int *isc) {
  int msc,i;
  int inm=1,ins=1,inc;
  unsigned int atom1,atom2,k;
  /*Choose an atom randomly in cell cn w/ indexed x-ref list indexR*/
  k=(unsigned int)(ran1(&RANSEED)*numinCell[cn]);
  /*add the starting point in indexR for cell cn*/
  k+=indexCell[cn];
  atom1=indexR[k];
  if(atom1<0 || atom1>=NUMINIT ) {
    printf("atom1 is forbidden #(%u). Return to continue\n",atom1);
  }
  *a1=atom1;
  msc=IP[atom1]; /*msc is initially the subcell atom atom1 is in */
  if(numinSubCell[msc]<2) {
    /*If there is not another atom to collide with in subcell */
    do { /*Find another subcell in cell that has an atom*/
      /*coll3() already checked numinCell>1 before calling select() */
      inc=inm*ins;
      ins=(-ins);
      inm++;
      msc+=inc;
    }while((msc<0||msc>=NSC)||(isc[msc]!=cn)||(!numinSubCell[msc]));
  }
  /* Now choose 2nd atom from subcell msc which are not atom1*/
  if(numinSubCell[cn]==1) {
    k=0;
    atom2=indexR[k];
  }
```

```
  else
    do {
      k=(int)(ran1(&RANSEED)*numinSubCell[msc]);
      k+=indexSubCell[msc];
      atom2=indexR[k];
    }while(atom2==atom1);
  if(atom2<0 || atom2>=NUMINIT) {
    printf("atom2 is forbidden number);
    getchar();
  }
  *a2=atom2;
}
/************ Function index3 *******************************/
/*******The atoms are arranged in order of cells, and
 within cells in order of subcells***********/
int index3(float **pp, float **pv, unsigned int *numinCell,
     unsigned int *indexCell, unsigned int *numinSubCell,
 unsigned int *indexSubCell, unsigned int *indexR,
 unsigned int *isc, int *gone){
  int i,j,msc,m,NUMPART=0,nc;
  /* First set "number of atoms in cell" to 0 for all cells */
  for(i=0;i<NC;i++)
    numinCell[i]=0;
  /* Same for Subcells */
  for(i=0;i<NSC;i++)
    numinSubCell[i]=0;
  totOort=0; /*Reset global totOort  */
  /** Count atoms in Cells and Subcells **/
  for(i=0;i<NUMINIT;i++) {
    if(oort[i]==0) { /* If atom is still in trap and in bins*/
      msc=IP[i];
      nc=isc[msc];
      numinSubCell[msc]++;
      numinCell[nc]++;
      NUMPART++;
    }
    else if (oort[i]==1) {
      totOort++;
    }
  }
 /*Setup array of start address in indexR for cells and subcells*/
  m=0;
  for(i=0;i<NC;i++) {
    indexCell[i]=m;
    m+=numinCell[i];
  }
  m=0;
  for(i=0;i<NSC;i++) {
    indexSubCell[i]=m;
    m+=numinSubCell[i];
    numinSubCell[i]=0;
  }
  /* Set up the cross-reference array  **/
  for(i=0;i<NUMPART;i++) {
    msc=IP[i];
    j=indexSubCell[msc]+numinSubCell[msc];
    numinSubCell[msc]++;
    indexR[j]=i;
```

```
  }
}
void move3(float **pp, float **pv,unsigned int *isc,int *gone) {
  static int orbitOutOfRange=0,firsttime=1,totgone=0;
  static double C[3],Sw[3],Sow[3];
  int i,j,tempint;
  float k1p,k1v,k2p,k2v,x,y,z,pold,temp;
  if(firsttime) {
    firsttime=0;
    for(i=0;i<3;i++) {
      C[i]=cos(W[i]*DT);
      Sow[i]=sin(W[i]*DT)/W[i];
      Sw[i]=sin(W[i]*DT)*W[i];
    }
  }
  /** Move atom through their orbit one DT */
  for(j=0;j<NUMINIT;j++) {
    if(oort[j]!=-1) { /* If atom is still in trap */
      for(i=0;i<3;i++) {
/** This is particular to case of harmonic trap.  For general
potential use Runge-Kutta or other reasonably energy
 conserving integrator **/
        pold=pp[j][i];
      pp[j][i]=pp[j][i]*C[i] +  pv[j][i]*Sow[i];
      pv[j][i]=pv[j][i]*C[i] -  Sw[i]*pold;
      }
      /* (Re-)Assign subcell number to atom now that it's moved*/
      if ( (tempint=assignSubCell(pp[j])) < 0) {
      tempint=(-tempint);
      if(oort[j]==0)  {
        if(!gone[j]) {
          printf("Atom #%d out of range in orbit for 1st time\n",j);
          totgone++;
          printf("%d atoms have at some point left bins\n",totgone);
          gone[j]=1;
        }
      }
      oort[j]=1;
      }
      else
      oort[j]=0;
      IP[j]=tempint;  /*IP[atom#] is subcell atom is in */
    } /* End of (if oort[j]!=-1) */
  } /* end of (for(j=0;j<NUMPART;j++) */
}
double ranvel(double *u, double *v, double vmp) {
  double A,B;
/*--generates two random velocity components u and v
 in an equilibrium gas with most probable speed vmp*/
  A=sqrt(-log(ran1(&RANSEED)));
  B=6.283185308*ran1(&RANSEED);
  *u=A*sin(B)*vmp;
  *v=A*cos(B)*vmp;
  return *u;
}
/*** The memory allocation routines, adapted
```

```
from Numerical Recipes, Press et. al */
int *newintarray(long length) {
  int *v;
  v=(int *)malloc((size_t)(length*sizeof(int)));
  if(v==NULL) {
    printf("Could not allocate integer array of length %ld\n",
        length);
    exit(-2);
  }
  return v;
}
unsigned int *newunsignedintarray(long length) {
  unsigned int *v;
  v=(int *)malloc((size_t)(length*sizeof(unsigned int)));
  if(v==NULL) {
    printf("Could not allocate unsigned int array of length %ld\n",
       length);
    exit(-2);
  }
  return v;
}
float *newfloatarray(long length) {
  float *v;
  v=(float *)malloc((size_t)(length*sizeof(int)));
  if(v==NULL) {
    printf("Could not allocate float array of length %ld\n",
      length)
    exit(-2);
  }
  return v;
}
float **newfloatmatrix(long rows, long columns) {
/* Allocated array range pp[0..rows-1][0..columns-1] */
  float **pp;
  int i,j;
/* Allocate some memory for array of pointers to rows*/
  pp=(float **)malloc((size_t)(rows*sizeof(float*)));
  if(!pp){
    printf("Couldn't allocate pp at pointer to rows level\n");
    exit(-1);
  }
  pp[0]=(float *)malloc((size_t)(columns*rows*sizeof(float)));
  if(!pp[0]) {
    printf("Couldn't allocate pp at actual rows level\n");
    exit(-1);
  }
  for(i=1;i<rows;i++)
    pp[i]=pp[i-1]+3;
  for(i=0;i<columns;i++)
    for(j=0;j<rows;j++)
      pp[i][j]=0;
  return pp;
}
int assignSubCell(float *p) {
  int i,j,k,i2,m,msc;
  static int temp=0;
```

```
  static int firsttime=1;
  int flag=1;
  /*j is x-cell column*/p/*j is x-cell column*/
  j=(int)floor( (p[0]-cgxmin[0])/cwx);
  if(j>NCX-1) {  /* Just to make sure */
    flag=-1;
    j=NCX-1;
  }
  if(j<0) {
    flag=-1;
    j=0;
  }
  /* Assign y-coord and find 'y-cell row' */
  k=(int)floor( (p[1]-cgymin[0])/cwy); /*k is y-cell row*/
  if(k>NCY-1) { /* Just to make sure */
    k=NCY-1;
    flag=-1;
  }
  if(k<0) {
    k=0;
    flag=-1;
  }
  /* Assign z=coord and find  z-cell slice */
  i2=(int)floor( (p[2]-cgzmin[0])/cwz );  /*i2 is z-cell slice */
  if(i2>NCZ-1){ /* Just to make sure */
    i2=NCZ-1;
    flag=-1;
  }
  if(i2<0) {
    i2=0;
    flag=-1;
  }
  m=i2*NCX*NCY + k*NCX + j; /*Cell Number*/
  if(m<0) { /* This shouldn't be able to happen */
    printf("Unexpected m<0 in assignSubCell\n");
    m=0;
  }
  if(m>NC) {
    printf("Unexpected m>NC in assignSubCell\n");
    printf("i2=    m=NC;
  }
  i2=(int)(((p[0]-cgxmin[m])/cwx)*((float)NSCX-0.001));
    j=(int)(((p[1]-cgymin[m])/cwy)*((float)NSCY-0.001));
  k=(int)(((p[2]-cgzmin[m])/cwz)*((float)NSCZ-0.001));
  msc=k*NSCX*NSCY+j*NSCX+i2+NSCX*NSCY*NSCZ*m; /*subcell number*/
  if(msc<0) {
    msc=0;
  }
  if(msc>NSC)
    msc=NSC;
  return (flag)*msc;
}
```

Bibliography

[1] M. H. Anderson, J. R. Ensher, M.R. Matthews, C. E. Wieman, and E. A. Cornell, Science **269**, 198 (1995).

[2] K. B. Davis, M. O. Mewes, M. R. Andrews, N. J. vanDruten, D. S. Durfee, D. M. Kurn, and W. Ketterle, Phys. Rev. Lett. **75**, 3969 (1995).

[3] R. A. Boyd. A Cryogenic Trap for Neutral Atoms. Doctoral thesis, California Institute of Technology, 1997.

[4] E. Tiesinga, B. J. Verhaar, and H. T. C. Stoof, Phys. Rev. A **47**, 4114 (1993).

[5] J. Söding, D. Guéry-Odelin, P. Desbiolles, G. Ferrari, and J. Dalibard, Phys. Rev. Lett., **80**, 1869 (1998).

[6] P. D. Lett, W. D. Phillips, S. L. Rolstron, C. E. Tanner, R. N. Watts, and C. I. Westbrook, J. Opt. Soc. Am. B **6**, 2084 (1989).

[7] J. Dalibard and C. Cohen-Tannoudji, J. Opt. Soc. Am. B **6**, 2023 (1989).

[8] P. A. Willems. Studies of Magneto-Optically and Magnetostatically Trapped Cesium in a Cryogenic Vacuum Apparatus. Doctoral thesis, California Institute of Technology, 1995.

[9] O. J. Luiten, H. G. C. Werij, I. D. Setija, M. W. Reynolds, T. W. Hijmans, and J. T. M. Walraven, Phys. Rev. Lett. **70**, 544 (1993); J. M. Doyle, J. C. Sandberg, I. A. Yu, C. L. Cesar, D. Kleppner, and T. J. Greytak, Phys. Rev. Lett. **67**, 603 (1991), and references therein.

[10] K. Helmerson, A. Martin, and D. E. Pritchard, J. Opt. Soc. Am. B **9**, 483 (1992).

[11] S. Gilbert and C. Wieman, Phys. Rev. A **34**, 792 (1986).

[12] K. B. MacAdam, A. Steinbach, and C. Wieman, American Journal of Physics **60**, 1098 (1992).

[13] K. G. Libbrecht and J.L. Hall, Rev. Sci. Instrum. **64**, 2133 (1993).

[14] V. I. Balykin, V. S. Letokhov, and A. I. Sidorov, Opt. Commun. **49**, 238 (1984).

[15] M. Prentiss and A. Cable, Phys. Rev. Lett. **62**, 1354 (1989).

[16] J. Prodan, A. Migdall, W. D. Phillips, I. So, H. Metcalf, and J. Dalibard, Phys. Rev. Lett. **54**, 992 (1985).

[17] Thomas E. Barret, Samuel W. Dapore-Schwartz, Mark D. Ray, and Gregory P. Lafyatis, Phys. Rev. Lett. **67**, 3483 (1991).

[18] J. R. Yeh, B. Hoeling, and R. J. Knize, Phys. Rev. A **52**, 1388 (1995).

[19] M. Zhu, C. W. Oates, and J. L. Hall, Phys. Rev. Lett. **67**, 49 (1991).

[20] Balykin and V. I. Mushin, JETP Lett. **29**, 560 (1979).

[21] W. Ertmer, R. Blatt, J. L. Hall, and M. Zhu, Phys. Rev. Lett. **54**, 996 (1985).

[22] R. N. Watts and C. E. Wieman, Optics Letters, **11**, 291 (1986).

[23] D. Sesko, C. G. Fan, and C. E. Wieman, J. Opt. Soc. Am. B **5**, 1225 (1988).

[24] C. C. Bradley, J. G. Story, J. J. Tollet, J. Chen, N. W. Ritchie, and R. G. Hulet, Optics Letters **17**, 349 (1992).

[25] O. Schmidt, K.M. Knaarm, R. Wynands, and D. Meschede, Applied Physics B **59**, 167 (1994).

[26] C. Cohen-Tannoudji, J. Dupont-Roc, and G. Grynberg, *Atom-Photon Interactions: Basic Processes and Applications* (John Wiley and Sons, New York, 1992).

[27] C. G. Townsend, N. H. Edwards, C. J. Cooper, K. P. Zetie, and C. J. Foot, Phys. Rev. A **52,** 1423 (1995).

[28] P. S. Julienne and Jacques Vigué, Phys. Rev. A **77**, 4464 (1991).

[29] L. D. Landau and E. M. Lifshitz, *Quantum Mechanics (Non-Relativistic Theory)* (Pergamon Press, 1977).

[30] C. R. Monroe, E. A. Cornell, C. A. Sackett, C. J. Myatt, and C. E. Wieman, Phys. Rev. Lett. **70**, 414 (1993).

[31] B. Verhaar, K. Gibble, and S. Chu, Phys. Rev. A **48**, R3429 (1993).

[32] K. Gibble, S. Chang, and R. Legere, Phys. Rev. Lett. **75**, 2666 (1995).

[33] M. Arndt, M. Ben Dahan, D. Guéry-Odelin, M. W. Reynolds, and J. Dalibard, Phys. Rev. Lett. **79,** 625 (1997).

[34] L. D. Landau and E. M. Lifshitz, *Mechanics* (Pergamon Press, 1976), §27.

[35] C. R. Monroe. Experiments with Optically and Magnetically Trapped Cesium Atoms. Doctoral thesis, University of Colorado, 1992.

[36] Kendall B. Davis, Marc-Oliver Mewes, Michael A. Joffe, Michael R. Andrews, and Wolfgang Ketterle, Phys. Rev. Lett. **74**, 5202 (1995).

[37] N. R. Newbury, C. J. Myatt, and C. E. Wieman, Phys. Rev. A **51**, R2680 (1995).

[38] N. R. Newbury, C. J. Myatt, E. A. Cornell, and C. E. Wieman, Phys. Rev. Lett. **74**, 2196 (1995).

[39] W. Petrich, M. H. Anderson, J. R., Ensher, and E. A. Cornell, Phys. Rev. Lett. **74,** 17 (1995).

[40] W. Ketterle and N.J. van Druten, Advances in Atomic Molecular and Optical Physics **37**, 181 (1996).

[41] H. F. Hess, Phys. Rev. B. **34**, 3476 (1986).

[42] N. Masuhara, J. M. Doyle, J. C. Sandberg, D. Kleppner, T. J. Greytak, H. F. Hess, and G. P. Kochanski, Phys. Rev. Lett. **61**, 935 (1988).

[43] C. J. Myatt. Bose-Einstein Condensation Experiments in a Dilute Vapor of Rubidium, Doctoral theis, University of Colorado, 1997.

[44] P. A. Willems and K. G. Libbrecht, Phys. Rev. A **51**, 1403 (1995).

[45] F. Reif, *Fundamentals of Satistical and Thermal Physics* (McGraw-Hill Book Company, 1965).

[46] K. Gibble and S. Chu, Phys. Rev. Lett. **70**, 1771 (1993).

[47] Huang Wu and Christopher J. Foot, J. Phys. B **29,** L321 (1996).

[48] Ki-Hwan Kim, Kwan-Il Lee, Heung-Ryoul Noh, Jong-An Kim, and M. Ohtsu, International Quantum Electronics Conference, May 1998.

[49] G. A. Bird, *Molecular Gas Dynamics and the Direct Simulation of Gas Flows*, (Clarendon Press, Oxford, 1994).

[50] C. J. Myatt, N. R. Newbury, R. W. Ghrist, S. Loutzenhiser, and C. E. Wieman, Opt. Lett. **21,** 290 (1996).

[51] R. S. Williamson, P. A. Voytas, R. T. Newell, and T. Walker, Optics Express, to be published.

[52] K. Gibble, S. Chang, R. Legere, Phys. Rev. Lett. **75,** 2666 (1995).

[53] Z. T. Lu, K. L. Corwin, M. J. Renn, M. H. Anderson, E. A. Cornell, and C. E. Wieman, Phys. Rev. Lett. **77**, 3331 (1996).

[54] P. J. Leo, E. Tiesinga, P. S. Julienne, D. K. Walter, S. Kadlecek, and T. G. Walker, Phys. Rev. Lett., to be published.

[55] E. Riis, D. S. Weiss, K. A. Moler, and S. Chu, Phys. Rev. Lett. **64**, 1658 (1990).

[56] K. I. Lee, J. A. Kim, H. R. Noh, and W. Jhe, Optics Letters **21**, 1177 (1996).

[57] C. M. VanAtta, *Vacuum Science and Engineering* (McGraw-Hill, New York, 1965).

[58] T. Hänsch and A. Schawlow, Opt. Commun. **13**, 68 (1975).